CFD Modelling and Experimental Testing of Thermal Calcination of Kaolinite Rich Clay Particles - An Effort towards Green Concrete

Gebremariam, Abraham Teklay

Publication date:
2015

Document Version
Publisher's PDF, also known as Version of record

CFD MODELING AND EXPERIMENTAL TESTING OF THERMAL CALCINATION OF KAOLINITE RICH CLAY PARTICLES: AN EFFORT TOWARDS GREEN CONCRETE

Abraham Teklay Gebremariam

Dissertation submitted to the faculty of Engineering and Science
at Aalborg University in partial fulfillment of the
requirements for the degree of

DOCTOR OF PHILOSOPHY

Aalborg University
Department of Energy Technology
Aalborg, Denmark
November 2015

CFD modeling and experimental testing of thermal calcination of kaolinite rich clay particles–An effort towards green concrete

Printed in Denmark by Uniprint

ISBN: 978-87-92846-51-8

AALBORG UNIVERSITY
Department of Energy Technology
Pontoppidanstræde 101
Aalborg East, DK-9220
Denmark

"If we knew what we were doing, it wouldn't be called research"

Albert Einstein.

Abstract

Cement industry is one of the major industrial emitters of greenhouse gases, generating 5-7% of the total anthropogenic CO_2 emissions. Consequently, use of supplementary cementitious materials (SCM) to replace part of the CO_2-intensive cement clinker is an attractive way to mitigate CO_2 emission from cement industry. SCMs based on industrial byproducts like fly ashes and slags are subject to availability problems. Yet clays are the most ubiquitous material on earth's crust. Thus, properly calcined clays are a very promising candidates as SCMs to produce green cements. Calcination at inappropriately high temperatures or long retention time will not only waste energy but also decrease the reactivity of the calcines due to possible recrystallization of the reactive phase into a stable crystalline phase. Therefore, it is very crucial to achieve an in-depth understanding of the calcination processes in a calciner and develop a useful tool that can aid in the design of a smart clay calcination technology, which makes the major objective of this study.

In this thesis, a numerical approach is mainly used to investigate the flash calcination of clay particles. A transient one-dimensional particle model which fully addresses not only the particle-ambient flow interaction but also the intra-particle processes has been successfully developed in a C++ program to examine calcination of clay particles suspended in a hot gas. The calcination process is also numerically studied using gPROMS (a general PROcess Modeling System) software. The model results from both C++ and gPROMS software show good similarity. Various experiments have been performed to derive key kinetic data, to collect data from a gas suspension calciner (GSC), and to characterize the calcines obtained under different calcination conditions, which are either provided to the numerical model as inputs or as database for model validation.

The model is able to reliably predict the temperature and residence time at which a given clay material attains optimum composition of the required material, metakaolinite. For kaolinite rich clay particles with mean particle size of 13.74 µm in diameter, moderate calcination temperatures (1173–1200 K) tend to display optimum amount of metakaol–

inite in a fraction of seconds with less risk of further phase transformation. High calcination temperatures (>1300 K), however, deplete the amount of metakaolinite and promote further recrystallization of metakaolinite into undesired mullite phase that influences pozzolanic property of calcines negatively. Different indicators have been used to spot the optimum pozzolanic property of the calcined clay material, among which is the density of calcines. By using the variation in density of calcines, an optimum residence time has been marked. At this time the calcines display a minimum density that corresponds to the most dehydroxylated calcines. The behavior of flash calcined kaolinite rich clays has also been examined experimentally. The composition and property of calcines observed experimentally supports model prediction. The agreement between model and experimental results confirms the validity of the model.

The optimum calcination parameters predicted in this study are crucial not only to maximize the yield of the desired product but also minimize the energy consumption during operation. Thus, the experimentally validated calcination model and simulation results can aid in an improved understanding of clay calcination process and also new conceptual design and optimization of clay calciners.

Dansk resume

Cementindustrien er en af de største udledere af drivhusgasser og producerer 5-7% af den totale menneskeskabte CO_2 emission. Som følge deraf er brug af alternative cementagtige materialer (Supplementary Cementitious Materials - SCM) en attraktiv måde at erstatte en del af de CO_2–intensive cement klinker og derved dæmpe udledningen af CO_2 fra cement industrien. SCMs baseret på industrielle biprodukter, såsom flyveaske og slagge, er vanskelige, da tilgængeligheden af produkterne er meget begrænsede. Derimod er ler det dominerende materiale i jordens skorpe, og derfor er korrekt kalcineret ler en meget lovende kandidat til SCM for producktion af grøn cement. Lerkalcinering bør finde sted indenfor et snævert temperatur- og tids-vindue: kalcinering ved uhensigtsmæssige høje temperature eller ved for lang retentionstid vil ikke bare være spild af energi, men også reducere produktets reaktionsevne, idet sandsynligheden for krystallisering af den reaktive fase over i en stabil krystallisk fase herved stiger. Det er derfor ekstremt vigtigt at opnå en dybdegående forståelse for kalcineringsprocessen for ler i en kalcinator, samt at implementere denne i et brugbart værktøj, som kan medvirke i design processen af "smart" ler kalcineringsteknologi, hvilket er hovedformålet med dette studie.

I afhandlingen er en numerisk tilgang hovedsageligt blevet brugt til at undersøge flash kalcinering af ler partikler. En transient endimensional partikelmodel, som udførligt kan håndtere såvel det partikel-nære flow som de intra-partikulære processer, er blevet udviklet i et C++ program med det formål at undersøge kalcinering af lerpartikler opslemmet i en varm gas. Kalcineringsprocessen er endvidere blevet undersøgt numerisk ved brug af softwaren gPROMS (a general PROcess Modeling System) software. De modellerede resultater fra både C++ og gPROMS viste fremragende overensstemmelse. Et antal eksperimenter er blevet udført med henblik på at udlede de væsenligste kinetiske data fra en suspensionskalciner (GSC) og til at karakerisere det kalcinerede ler opnået under forskellige kalcineringsprocesser. De kinetiske data er derefter enten givet til den numeriske model som input eller som en database for model validaering.

Modellen er i stand til pålideligt at kunne forudse temperatur og opholdstid, hvorved et givet lermateriale opnår den optimale sammensætning af det ønskede materiale, metakoalinit. For lerpartikler rige på kaolonit, med en gennemsnitlig størrelse på 13.74 µm i diameter, opnåedes maksimal kaolinit-indhold nærmest øjeblikkeligt ved moderate kalcineringstemperaturer på 1173-1200 K. Samtidig var dette en stabil tilstand, med minimal risiko for videre fasetransformation. Høje kalcinerings temperature (>1300 K) derimod gav meget lave kaolinit-niveauer og gav desuden anledning til øget krystallisering af metakaolinit hen imod den uønskede mullit fase, som påvirker det kalcinerede lers pozzolaniske egenskaber i en negativ retning. Forskellige indikatorer er blevet benyttet til at finde den optimale pozzolaniske egenskab af det kalcinerede ler materiale, blandt hvilke er densiteten af den kalcinerede ler. Ved at benytte en variation i densiteten af det kalcinerede ler, har det været muligt at fastslå en optimal opholdstid. Til dette tidspunkt viser det kalcinerede ler en minimumsdensitet , hvilket svarer til det mest hydroxylerede kalcinerede ler. Det flash kalcinerede og kaolinit-rige ler er også blevet undersøgt eksperimentelt. Sammensætningen og egenskaber af det kalcinerede ler fra eksperimenterne understøtter de forudsagte resultater fra modellen. Overensstemmelsen imellem modellen og de eksperimentelle resultater bekræfter validiteten af modellen.

De optimale kalcineringsparametre fundet i dette studie er signifikante ikke bare for at kunne maksimere afkastet af en det ønskede produkt, men også i forhold til at minimere energiforbruget under drift. Således er det vist, at resultaterne fra den eksperimentelt validerede kalcineringsmodel og simuleringer kan medvirke til en forbedret forståelse af ler kalcinering samt i et nyt conceptuel design og optimering af ler kalcinatorer.

Acknowledgements

This work constitutes the effort, influence and inspiration of many individuals whom I would like to acknowledge. First and above all, I praise and thank GOD who bestowed us the power for learning, searching and performing.

Next, I would like to express my deepest gratitude to my principal supervisor Associate Professor Chungen Yin for his invaluable time, encouragement and support invested during the supervision of this project. I am also heartily thankful to my co-supervisor Professor Lasse Rosendahl for his kind advice and discussion.

I am indebted to the persons who actively participated in this research. Therefore, I would take this opportunity to thank Martin Bøjer, Anicka Adelsward, Lea Lindequist and Klaus Hjuler for their helpful discussion and suggestions.

My appreciation and admiration also extends to FLSmidth A/S for providing office and other facilities during my stay in Valby, Copenhagen. Also special thanks to the people at FLSmidth research center in Dania who helped me during my laboratory experiments. I am also thankful to Thomas Søren at the Department of Mechanical and Production Technology for his support during TGA experiments. The same gratitude goes to Marie, Lars and Samuel for reading and commenting on the thesis.

There are many more who deserve my gratitude, far too many to list here. In general, I am truly grateful to all of my colleagues whom I have come to know during my stay at the university and have spent many memorable fun all together.

My sincere thanks also go to project partners Aalborg Portland and Arhus university (iNANO) for their discussion and feedback during the course of the project.

Lastly, I would like to express all my gratitude to my parents for their continuous love and encouragement; in particular to my beloved wife Hilina and my son Tobias, for their patience and understanding during the long hours spent at office.

Contents

List of Figures

List of Tables

Nomenclature

A_k	Frequency factor of k^{th} reaction	s^{-1}
A_{surf}	Particle surface area	m^2
B_i	Biot number	-
C_p	Specific heat	kJ/(kg·K)
D	Diffusion coefficient in pores	m^2/s
D_{AB}	Molecular diffusivity of gase A in B	m^2/s
D_{eff}	Effective Diffusivity	m^2/s
$D_{j,m}$	Diffusivity of species j in gas mixture	m^2/s
d_p	Pore diameter	m
E_k	Activation energy of k^{th} reaction	kJ/mol
$\triangle H_k$	Heat of k^{th} reaction	kJ/kg
h	Sensible enthalpy of gas mixture	kJ/kg
$h_{i,j}$	Sensible enthalpy of solid/gas species	kJ/kg
h_m	Mass transfer coefficient	m/s
h_T	Heat transfer coefficient	$W/(m^2 \cdot K)$
k_{eff}	Effective conductivity	W/(m·K)
k_g	Gas conductivity	W/(m·K)
k_s	Conductivity of solid	W/(m·K)
MW_i	Molecular weight of the i^{th} species	kg/kmol
n	Order of reaction	-
Nu	Nusselt number	-
P	Pressure	Pa
P_{atm}	Atmospheric pressure	Pa
Pe_m	Peclet mass transfer number	-
Pr	Prandtl number	-
$\dot{r}_k$	Rate of k^{th} reaction	$kg/m^3 \cdot s$
R	Universal gas constant	kJ/(mol·K)
Re	Reynolds number	-
R_p	Particle radius	m
Sc	Schmidt number	-

Sh	Sherwood number	-
S_h	Source/sink term in the energy equation	W/m^3
S_g	Source/sink term in the continuity equation	$kg/(m^3 \cdot s)$
$S_{y,j}$	Source/sink term in species transport equation	$kg/(m^3 \cdot s)$
t	Time	s
T	Temperature	K
T_{film}	Reference temperature of gas film	K
T_{rad}	Radiation temperature	K
T_s	Particle surface temperature	K
T_∞	Ambient gas temperature	K
$\mathbf{U}$	Physical velocity of gas	m/s
V	Particle volume	m^3
$W_{1/2}$	Half width of a peak	-
Y_j	Mass fraction of species j	-
$Y_{j,film}$	reference mass fraction of species j in the gas film	-
$Y_{j,s}$	Mass fraction of species j at particle surface	-
$Y_{j,\infty}$	Mass fraction of species j in the ambient gas	-

Greek letters

α	Degree of dehydroxylation	-
β	Mass ratio of crystal water in kaolinite	-
ε	Porosity	-
η	Permeability	m^2
θ	Heating rate	K/s
μ	Dynamic viscosity	$kg/(m \cdot s)$
ρ_i	Density of i^{th} species	kg/m^3
ρ_g	Gas density	kg/m^3
σ	Stefan-Boltzmann constant	$W/(m^2K^4)$
τ	Tortuosity	-
ϕ	Thiele number	-
ω	Particle emissivity	-

Subscripts

cr	Cristobalite
fw	Free water
kl	Kaolinite
mk	Metakaolinite

mu	Mullite
sil	Silica
sp	Spinel

Abbreviations

ACI	**A**merican **C**oncrete **I**nstitute
ASR	**A**lkali-**S**ilica **R**eactions
BDNLSOL	**B**lock **D**ecomposition **N**on **L**inear **SOL**ver
CFD	**C**omputational **F**luid **D**ynamics
DAE	**D**ifferencial-**A**lgebraic **E**quation
DASOLV	**D**ifferencial-**A**lgebraic equation **SOL**ver
DSC	**D**ifferential **S**canning **C**alorimetry
DTA	**D**ifferential **T**hermal **A**nalysis
DTG	**D**ifferential **T**hermo **G**ravimetry
FVM	**F**inite **V**olume **M**ethod
GHG	**G**reen **H**ouse **G**as
gPROMS	**g**eneral **PRO**cess **M**odeling **S**ystem
LECO	**L**aboratory **E**quipments **CO**mpany
ODE	**O**rdinary **D**ifferential **E**quation
PDE	**P**artial **D**ifferential **E**quation
SCM	**S**upplementary **C**ementitious **M**aterial
TDMA	**T**ri **D**iagonal **M**atrix **A**lgorithm
TGA	**T**hermo **G**ravimetric **A**nalysis

Mandatory page

Thesis title : CFD modeling and experimental testing of thermal calcination of kaolinite rich clay particles : An effort towards green concrete
Name of PhD student : Abraham Teklay Gebremariam
Name and title of supervisors : Chungen Yin, Associate Professor; Lasse Rosendahl, Professor
List of published papers:
Paper 1: **Abraham Teklay**; Chungen Yin; Lasse Rosendahl; Martin Bøjer.Calcination of kaolinite clay particles for cement production: A modeling study. Cement and Concrete Research 61-62 (2014), 11-19

Paper 2: **Abraham Teklay**; Chungen Yin; Lasse Rosendahl; Lea Lindequist Køhler. Experimental and modeling study of flash calcination of kaolinite rich clay particles in a gas suspension calciner. Applied Clay Science 103 (2015), 10-19.

Paper 3: **Abraham Teklay**; Chungen Yin; Lasse Rosendahl. Flash calcination of kaolinite rich clay and impact of process conditions on the quality of the calcines: A way to reduce CO_2 footprint from cement industry. (doi:10.1016/j.apenergy.2015.04.127, Applied Energy, 2015)

Conference Contributions:
• **Abraham Teklay**; Chungen Yin; Lasse Rosendahl. Modeling of calcination of single kaolinitic clay particle. Presented at the 8^{th} International Conference on Multifluid Flow (ICMF2013), Jeju, Korea, 2013
• **Abraham Teklay**; Martin Bøjer; Anicka Adelsward; Chungen Yin; Lasse Rosendahl. Simulation of flash dehydroxylation of clay particle using gPROMS: A move towards green concrete. Proceedings in The 6^{th} International Conference on Applied Energy, Taiwan, 2014; Energy procedia 61 (2014), 556-559

This present report combined with the above listed scientific papers has been submitted for assessment in partial fulfilment of the PhD degree. The scientific papers are not included in this version due to copyright issues. Detailed publication information is provided above and the interested reader is referred to the original published papers. As part of the assessment, co-author statements have been made available to the assessment committee and are also available at the Faculty of Engineering and Science, Aalborg University.

Chapter 1

Introduction

This chapter gives an overview of the significance of the study and defines the objectives and scope of the thesis. It also presents the methodology and approach used to arrive at the final conclusions, followed by contribution of the study.

1.1 Overview

Fueled by the current environmental concern and the ever increasing demand for cement, the present emission trends in cement industry need to be halted. The use of supplementary cementitious materials to offset a portion of cement powder in concrete has got paramount significance in lowering the environmental cost associated with the emission of greenhouse gases from cement production. With this respect, the current study finds a method of optimizing the pozzolanic reactivity of kaolinite rich clay particles that can be used as SCMs. Kaolinite being one of the most abundant clay mineral, its excellent pozzolanic properties has drawn renewed attention in cement and concrete industry. Calcination of kaolinite is among the popular methods to produce the metastable phase called metakaolinite, which has a particular mineralogical properties that can be utilized as a mineral admixture in cement and concrete production.

Well-calcined clay products especially metakaolines have shown pozzolanic activity equal to or higher than the well-known artificial pozzolans such as; fly ash, silica fume and blast furnace slag. The fact that most clay minerals are compositionally suitable to be used as pozzolanic materials is the starting point of the investigation.

1.2 Objectives and scope of thesis

One of the key visions of this project is to elaborate an innovative processes and know-how needed to convert the locally available clays into high-quality SCM products. The pozzolanic reactivity of such clays largely depends on the pyroprocessing or calcination conditions (e.g., temperature, residence time of clay particles in the calciner), as well as clay properties (e.g., type of clay, particle size distribution, morphology). With this respect, the key objective of this study is to find out how to obtain clay particles with the desired pozzolanic properties by smart calcination or pyroprocessing; so that these reactive clay products could be used as a partial clinker substitute to mitigate the emission of CO_2 from cement industries. While *Modeling* is the main workhorse of the study, supplemental laboratory tests and experiments are key inputs to validate the model.

The main scope of this PhD study is therefore:

- Develop a calcination model for single clay particle, which is able to simulate the heat transfer process and simultaneous changes in composition during thermal calcination
- Predict the spatial and temporal evolution of temperature and composition inside a clay particle of different size calcined under different conditions
- Validate the model experimentally by performing experiments in a pilot scale gas suspension calciner
- Propose optimum calcination conditions (temperature and residence time) that can be used to turn the clay material into useful SCM product

1.3 Methodology

This thesis focuses on the development of a numerical model to study the calcination process of kaolinite rich clays, and experimental examination of the clay material using TGA and pilot scale gas suspension calciner. The general approach is described briefly as follows:

Numerical model

One-dimensional transient particle model has been developed using C++ and gPROMS softwares. The major intention of using gPROMS software is to develop the calcination

model which later could be used to simulate results in a tubular reactor or combine the gPROMS calcination model with CFD to run simulation of gas suspension calciner. However, the use of gPROMS is suspended due to adjustments made by the project consortium. The results generated by gPROMS are used as a verification effort for the C++ results.

Generally, the model addresses the conversion of a kaolinite particle when inserted into a hot gas atmosphere. The process can be understood by considering a porous kaolinite clay particle, when suspended in the hot gas, heat is transferred to the particle surface by convection and radiation. As heat penetrates into the surface, different reactions and phase transformations commence causing the release of water vapor through the porous surface. In order to address this phenomena numerically, the particle has been discretized into a number of spherical cells, on each of which mass, momentum, energy and species conservation equations are numerically solved by using the finite volume method. The model reliably predicts the conversion and simultaneous changes in composition.

Experimental study

A number of experiments are carried out either to provide an input data to the model or experimental evidences for model validation. These experiments cover a wide scope of tests ranging from TGA to comprehensive flash calcination tests in a gas suspension calciner, including various characterization methods of the feed and the calcines.

TGA experiments are performed to collect kinetic parameters (E and A) which are vital inputs to the model. TGA tests are also used as part of model validation, where the conversion of the clay particle is compared with model prediction.

Calcination experiments are performed in a pilot scale gas suspension calciner, where flash calcines have been produced at different calcination conditions inside the GSC. The composition and property of the calcines has been further analyzed.

Characterization of the feed and calcines have been carried out using several methods. The composition and degree of dehydroxylation for the feed and calcines are investigated using X-ray diffraction (XRD) and LECO thermal analyzer, respectively. The amount of phases such as kaolinite, metakaolinite and mullite are compared with model predicted ones. Other relevant properties such as the PSD, the density and specific surface area of the feed and calcines are examined using laser diffraction, Gas Pycnometer and BET method, respectively. Experimental outputs such as the degree of dehydroxylation and the specific density are used to validate the model results.

1.4 Contribution of thesis

The contribution of this thesis is largely to elaborate an innovative process and know-how needed to convert the locally available materials, such as clays, into high-quality SCM products. The reactivity of clays largely depends on calcination conditions (e.g., temperature, residence time of clay particles in the calciner), as well as clay properties (e.g., type of clay, particle size distribution, morphology). The fundamental knowledge on these effects is understood by modeling the clay particle and simulating at different calcination conditions. With this regard, the major contributions of this thesis are:

- A comprehensive calcination model for kaolinite particle has been developed. The model considers several reactions such as dehydration, dehydroxylation and various phase transformations that may occur when the clay particle is heated.
- Optimum calcination path for the conversion of kaolinite to metakaolinite is predicted. Consequently, the time-temperature-transformation curve is derived.
- The composition of calcines has been experimentally characterized after the clay material has been being exposed to different calcination conditions in the GSC. The amount of different phases has been quantified with the aid of experimental techniques. Experimental results show reasonable agreement with model prediction.
- A comprehensive model-based sensitivity analysis of the impacts of the most important calcination conditions (such as, temperature and time); and clay particle properties (such as, particle size and kinetic parameters) has been carried out. Their impact on the property of the final product has been explained.

1.5 Thesis outline

This thesis is prepared as a collection of scientific papers produced during the entire PhD period. It is composed of 6 chapters which are described as follows;

Chapter 1 gives a general overview on the study and defines the scope and objectives of the thesis. It also lists the contribution of the thesis.

Chapter 2 presents a solid background on the production of cement and the significance of SCMs in alleviating CO_2 from cement industries. It also presents literature review on the calcination of clays, specifically on kaolinite rich clays. Finally, it reviews the available literature on modeling and experimental study on calcination of kaolinite rich clay particles.

Following the background and literature review, the details of a single particle calcination model are extensively discussed in **Chapter 3**. The mathematical approach and major assumptions are described at the beginning, then the governing equations and methods of discretization are explained.

Chapter 4 describes the experimental section where several tests are performed in order to determine the kinetic parameters of clay calcination, which are the main inputs of the model. Calcination tests in a pilot scale gas suspension calciner are presented along with characterization method of the calcines.

Chapter 5 is a summary of result and discussions. In this chapter, the major results of this project are discussed in relation to the objectives of the study and the existing literature. A brief discussion on model validation is made. Model predicted results are also discussed and the impacts of key factors in clay calcination (e.g., particle size, gas temperature and reaction kinetics) are also examined through a model-based sensitivity analysis.

Finally, the main conclusion and recommendations for future work are provided in **Chapter 6**.

Chapter 2

Background and literature review

This chapter presents the background on the production of cement and its impact on the environment. It also highlights the advantage of using of SCMs in reducing CO_2 footprint from cement industry. Finally, the efforts reported in literature to understand the calcination of kaolinite rich clays either by using models or through experimental study are reviewed.

2.1 Production of cement

Production of cement generally involves the following broad stages: quarrying and processing of raw materials; pyroprocessing to produce clinker; blending and grinding of clinker to cement and finally storage and packing.

Generally the raw materials are a mixture of minerals containing calcareous, siliceous, argillaceous, and ferriferous materials that mainly include limestone, marl and shale or clay, which are extracted from quarries. These materials are primarily crushed and milled before they are transported to the cement plant for storage and further conditioning. The raw materials, in controlled proportions, are ground and mixed together to form a homogeneous blend in fineness and composition. Figure 2.1 provides a typical production flowchart of Portland cement.

The minerals are transferred into the kiln system where the raw mix is fused at high temperatures to alter into new minerals with hydraulic properties. Prior to introducing the raw mix into the rotary kiln, it is pre-heated and calcined at the pre-calciners where the majority of heat source comes from the waste heat of rotary kiln.

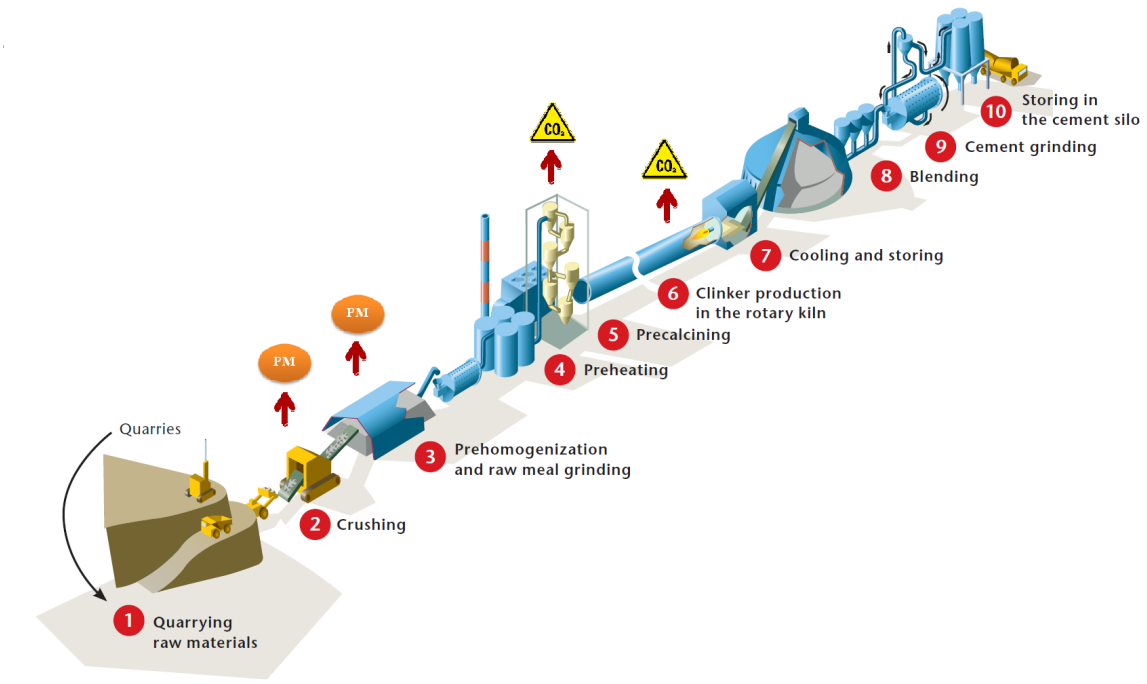

FIGURE 2.1: The production process of Portland cement showing the major pollution sites of carbon dioxide and particulate matter(PM).

The heart of the Portland cement manufacturing process is the pyroprocessing stage where the chemistry of the cement manufacturing process begins. This process transforms the raw mix into clinker through the process called calcination. At this stage of the process, calcium carbonates is decomposed to yield calcium oxide (CaO) and CO_2. This is followed by the clinkering process at the rotary kiln where the raw material mix enters the kiln at the elevated end in a counter current manner to the flow of fuels. As the feed materials are continuously and slowly moved down the kiln, the raw materials are changed to cementitious or hydraulic mineral called clinker, which is a product of high temperature reactions (typically $1673 - 1773K$) between calcium oxide, silica, alumina, and ferrous oxides. The hot clinker then falls onto a grate cooler where it is cooled rapidly by air.

The final step in the manufacturing of Portland cement is blending and grinding operations that transform clinker to finished Portland cement. Up to 5% gypsum or natural anhydrite is added to the clinker during grinding to control the cement setting time. At this stage, addition of other minerals (blast furnace slag, metakaolinite, fly ash or silica fume) could be accomplished to reduce the CO_2 footprint from the industry.

2.1.1 Impact of cement production on the environment

Most emissions that come out of cement industry are from the kiln system. The main constituents of the exit gas are oxides of nitrogen, oxides of sulfur and oxides of carbon generated due to process related chemical reactions and combustion of fuels. The emission of these gases is environmentally damaging. CO_2 being the major constituent of the exit gas, it is produced by two mechanisms:

1. Calcination of limestone or other calcareous materials at high temperature.

$$\underset{1\text{kg}}{CaCO_3} \rightarrow \underset{0.56\text{kg}}{CaO} + \underset{0.44\text{kg}}{CO_2}$$

2. Combustion of fuel during pyroprocessing that releases substantial quantities of CO_2.

As a result, cement industry is associated with the emission of large amounts of CO_2 from both calcination and combustion processes. Every kilogram of Portland cement generates 0.73–0.99 kilogram of CO_2 which comprises approximately 5-7% of total anthropogenic CO_2 emissions [Mehta, 2002]. When all greenhouse gas emissions generated by human activities are considered, the cement industry is responsible for approximately 3% of global emissions [Humphreys and Mahasenan, 2002; Mehta, 2002]. Figure 2.2 describes the global greenhouse gas emissions and contribution of cement industry [Humphreys and Mahasenan, 2002; Rehan and Nehdi, 2005].

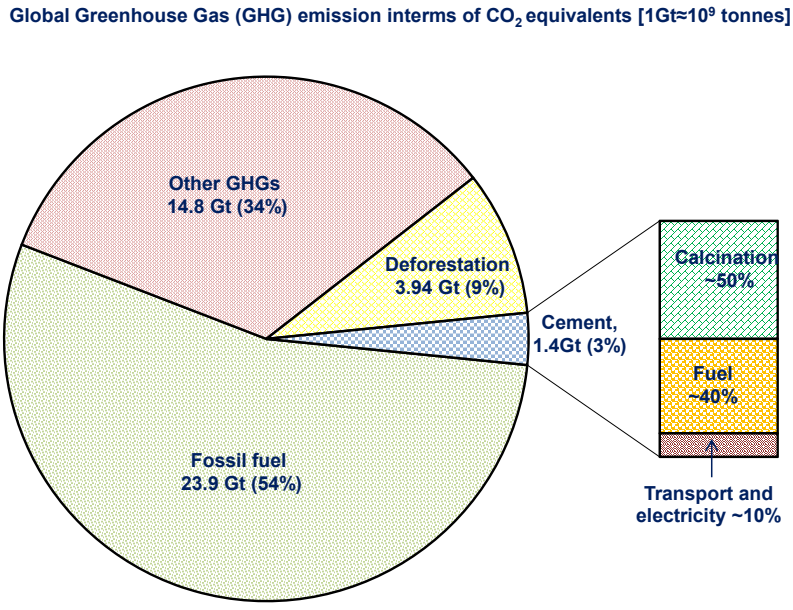

FIGURE 2.2: The global greenhouse gases emission in the year 2000 and contribution of cement industry [Rehan and Nehdi, 2005].

Like many other industrial activities, the cement industry needs to strictly comply with national and international emission abatement regulations. Moreover, with the drastic increase in Portland cement production foreseen in the future, the current cement industry is facing challenges of producing more sustainable and less energy intensive products without sacrificing the mechanical performance or durability of the end product. As a result, different strategies have been forwarded to alleviate CO_2 emission from cement industry [IEA, 2009], among them are, the use of alternative fuels, use of carbon capture and storage strategies and use of SCMs.

In this study the use of SCMs is of main interest, and hence, the use of natural or artificial pozzolans such as calcined clays are considered as a useful admixtures of Portland cement. The potential future of clay materials as SCM is not only because of its availability, but also due to its environmental advantage.

The use of metakaolinite as SCMs has been extensively studied in the literature [Arikan et al., 2009; Cassagnabère et al., 2010; He et al., 1994; Khatib et al., 2012; Said-Mansour et al., 2011; Salvador, 1995; Shvarzman et al., 2003; Tironi et al., 2012] and found that partial substitution of metakaolinite (up to $\sim$ 20% of clinker) plays a significant role in the production of green concretes without compromising the mechanical property and durability of the blended concrete. However, proper thermal activation of kaolinite clay is critical, because the above mentioned benefits are directly related to the amount metakaolinite in the calcined product.

2.2 Supplementary Cementitious Materials (SCMs)

The use of pozzolana along with Portland cement was originally practiced to reduce the cost of Portland cement. However, the mixture of pozzolana and Portland cement has got other interesting benefits such as inhibiting or suppressing the alkali-silica reactions that improve the durability of cement. In this regard, the construction of Friant dam in California in 1940 was a typical example proving the benefits of blending cement with natural pozzolan (Pumicite) to reduce the deterioration of concrete due to expansion [Hewlett, 1998].

The use of metakaolin blended concrete has also been practiced since 1960's to mitigate alkali-silica reactions and improve durability of concrete; with this regard, the construction of Jupia Dam in Brazil in 1962 using metakaolinite as a partial substitute of cement was a great success [Li et al., 2010].

The knowledge and the practice of substituting part of cement with SCMs has long been exercised for several decades, and still it is under investigation. One can easily perceive

the complexity of the subject as it still attracts the attention of many researchers and business firms.

SCMs are a group of materials that show either hydraulic or pozzolanic behavior, in such a way that it can set and harden in the presence of water by forming cementitious products in a hydration reaction [Massazza, 1993]. This group of materials embraces a large number of materials which vary widely in terms of origin, mineralogical composition, and typical particle characteristics. Typical examples of such materials are fly ash, silica fume, blast furnace slag, metakaolin, rice husk ash and natural pozzolans.

SCMs could be categorized in two broad distinctions: materials of natural origin (natural SCMs) and materials of man-made or artificial origin (artificial SCMs). Natural SCMs consist materials that can be used in their naturally occurring form after being conditioned by sieving and grinding processes. Typical examples are volcanic ash or pumicite, shales, tuffs, and some diatomaceous earth.

Artificial SCMs includes materials which have undergone structural modifications as a consequence of manufacturing or production processes. They can be produced deliberately by thermal method, for instance by thermal activation of kaolinite to obtain metakaolin, or can be obtained as waste or by-products from high temperature processes such as blast furnace slags, fly ashes or silica fume.

SCMs such as fly ash, slag and calcined clays are the most promising materials as cement admixture. Among all SCMs, those based on calcined clay are the future materials as cement admixture; primarily because of their availability and additionally they modify the performance and durability of a concrete [Cassagnabère et al., 2010; Sabir et al., 2001].

Today, artificial SCMs such as metakaolinite are enjoying a renaissance as SCMs in cement industry and may replace part of the clinker not only to mitigate CO_2 footprints from cement production but also to enhance the performance of the concrete by decreasing the deleterious alkali-silica reactions [Cassagnabère et al., 2010; Lothenbach et al., 2011; Sabir et al., 2001].

2.2.1 The need for SCMs

There has been a continuous search for material admixtures that can improve the workability, strength and durability of a concrete. Recently, due to the strict air pollution controls and regulations imposed on cement industry, an alternative material search has primarily focused on materials that can be utilized to reduce CO_2 footprint from cement industry.

In addition to the environmental benefits, some of the broad benefits of incorporating SCMs as partial cement replacement are; increased compressive strength, reduced segregation, reduced permeability, mitigation of alkali-silica reactions and enhanced workability. It has also been shown that using multiple SCMs as a cement admixture appear to have synergistic effect in the concrete [Shehata and Thomas, 2002; Thomas et al., 1999]. This is because of the chemical and physical differences of each SCM additive stimulate different reactions in the concrete, granting a unique property of high-performance concretes. Table 2.1 presents the general effect of SCMs on the property of hardened concrete [Dam, 2013].

TABLE 2.1: Effects of SCMs on the properties of hardened concrete

Property	Fly ash(Type C)	Slag	Silica fume	Metakaoline
Early strength	↔	↓	↑↑	↑↑
Long term strength	↑	↑	↑↑	↑↑
Permeability	↓	↓	↓↓	↓↓
Chloride ingress	↓	↓	↓↓	↓↓
ASR	↕	↓↓	↓	↓
Sulfate resistance	↕	↑↑	↑	↑
Freezing and thawing	↔	↔	↔	↔
Abrasion resistance	↔	↔	↔	↔
Drying shrinkage	↔	↔	↔	↔

• **KEY**
↓ Reduced
↓↓ Significantly reduced
↑ Increased
↑↑ Significantly increased
↔ No significant change
↕ Effect varies

One major concern regarding the use of SCMs may be the initial cost associated with production the SCM-cement blend. Specially using metakaolinite as SCM may surge the overall cost of the concrete, as calcination of this material incurs additional cost on the blended cement. Usually the initial cost of a concrete containing metakaolinite additive is expected to increase. The real economic savings are obtained over the lifecycle, as the enhancements in ultimate strength, and durability often result an improved long-term performance.

2.2.2 Pozzolanic reactivity

A Pozzolan is generally defined in ACI 116R as "..a siliceous or siliceous and aluminous material which, in itself, possesses little or no cementitious value but which will, in finely divided form and in the presence of moisture, react chemically with calcium hydroxide (lime) at ordinary temperature to form compounds possessing cementitious properties"

[Tikalsky et al., 2001]. Hence, the term pozzolana includes all those inorganic materials, either natural or artificial, which harden in water when mixed with calcium hydroxide. Generally, it embraces a large number of very different materials in terms of origin, composition and structure.

Pozzolanic reactivity, therefore, covers all reactions occurring among the active constituents of pozzolanas, lime and water. Pozzolanic reactivity of SCMs is characterized by the reaction between siliceous or aluminosiliceous material in the SCM with calcium hydroxide (a reaction product from the hydration of Portland cement), forming calcium silicate hydrate and other cementitious compounds that have a positive impact on the long-term properties of the hardened concrete.

2.3 Kaolinite

Kaolin is a fine, white, clay mineral that has traditionally been used in the manufacturing of porcelain. Kaolinite is the mineralogical term that is applicable to kaolin clays composed of hydrated aluminum silicates. Its structural formula is $Al_2Si_2O_5(OH)_4$ with theoretical composition of 46.54% SiO_2, 39.5% Al_2O_3 and 13.96% H_2O. The shape of a perfectly ordered kaolinite crystal is pseudo-hexagonal, but its crystallinity may range from a highly crystalline to a poorly ordered crystal [Prasad et al., 1991].

Kaolinite is the most prominent 1:1 type of phyllosilicate clay mineral. It has flake(flat) type morphology due to the arrangement of atoms in the structure. The basic structure is made through the arrangement of two layers: the tetrahedral and octahedral layer. Each tetrahedron consists Si^{4+} cation coordinated to four oxygen atoms that are linked to adjacent tetrahedra by sharing three oxygen atoms at the corner; while the octahedron consist Al^{3+} cations surrounded by six hydroxyl groups. The free corners of the tetrahedral sheet connect with the octahedral sheets to form a common plane or a single layered structure. The sheet of atoms are stacked on top of each other in Tetrahedral-Octahedral (TO) fashion to form a layered structure. These layers, in turn, are held together by hydrogen bonding between hydroxyls of the octahedral layer and oxygen of the tetrahedral layer to form a repeating pattern of kaolinite clay structure as shown in Figure 2.3.

Three fourth of the hydroxyl groups in the kaolinite structure lie in the interlamellar space, while one fourth lie in the intralamellar space between the silica and alumina sheets [Slade and Davies, 1991]. When kaolinite gets heated at temperatures above 700 K, sequential loss of hydroxyls has been observed [Slade et al., 1991]; those hydroxyls

situated at the interlamellar space being easier to get removed than the intralamellar ones.

Kaolinite has got many interesting properties such as fine particle size, non-abrasiveness, chemical stability and low viscosity at high solid content. Moreover, its structure exhibits very little shrinkage and swelling [Grim, 1953]. Owing to these properties, it has got several industrial applications notably as a filler in paper, rubber and paint industry [Murray, 1963]. Furthermore, it can be utilized as supplementary cementitious material in cement and concrete industry after being properly calcined [Sabir et al., 2001].

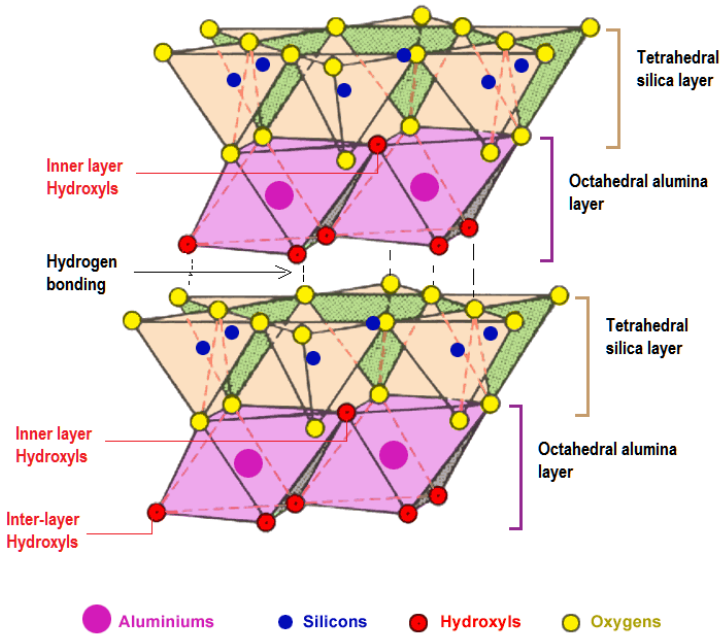

FIGURE 2.3: The arrangement of tetrahedral silica and octahedral alumina layers to form kaolinite structure

In a comparative study to assess the reactivity of different clays, it turns out that thermal activation of kaolinite displays high pozzolanic reactivity compared to other clays such as montmorillonite and illite [Ambroise et al., 1985; Fernandez et al., 2011]. Consequently, Kaolinite has been the interest of many researchers in the cement area, as it can be thermally activated to produce the highly reactive pozzolanic material, metakaolinite.

2.3.1 Calcination of kaolinite

Thermal decomposition of kaolinite at moderate temperature (700-1000 K) yields amorphous structured material called metakaolinite ($Al_2Si_2O_7$), a material that offers good properties as supplementary cementitious material [He et al., 1994; Shvarzman et al., 2003]. Thermal exposure beyond a definit point will result the formation of spinel-type

($Al_4Si_3O_{12}$) of phase along with amorphous silica, after which crystalline phases of mullite ($Al_6Si_2O_{13}$) and cristobalite (SiO_2) form. The appearance of crystalline phases may cause a decline in pozzolanic reactivity of the calcined material [Sabir et al., 2001].

A complete structural transformation of kaolinite mineral during thermal treatment passes through a sequence of reactions [Brindley and Nakahira, 1958; Ptáček et al., 2011], that occur at different temperatures. The whole transformation may be represented by the following reaction scheme:

$$H_2O(l, free) \xrightarrow{373K} H_2O(g) \quad \triangle H = -2242(\text{kJ/kg}) \tag{2.1}$$

$$Al_2Si_2O_5(OH)_4(Kaolinite) \xrightarrow{700-1000K} Al_2Si_2O_7(Metakaolinite) + 2H_2O \quad \triangle H = -632(\text{kJ/kg}) \tag{2.2}$$

$$2(Al_2Si_2O_7) \xrightarrow{1000-1300K} Al_4Si_3O_{12}(Spinel) + SiO_2 \quad \triangle H = +230(\text{kJ/kg}) \tag{2.3}$$

$$3(Al_4Si_3O_{12}) \xrightarrow{\geq 1300K} 2(Al_6Si_2O_{13})(Mullite) + 5SiO_2 \quad \triangle H = +84(\text{kJ/kg}) \tag{2.4}$$

$$SiO_2(Amorphous\ \ silica) \xrightarrow{\geq 1473K} SiO_2(Cristobalite) \quad \triangle H = +42(\text{kJ/kg}) \tag{2.5}$$

With regard to this study, the first two reactions, namely evaporation and dehydroxylation are the most important reactions. Especially, the dehydroxylation reaction is the one that needs to be optimized as the most pozzolanic material (metakaolinite) is obtained at this stage. The remaining reactions that may occur at or beyond 1300 K are phases transformations that deplete the amount of metakaolinite into spinel and mullite phases; and hence need to be controlled.

Generally the above reactions are characterized by complex solid state reactions that are influenced by the crystallinity of the kaolinite sample [Cabrera and Eddleston, 1983], particle size [Lahiri, 1980], vapor pressure [Brindley et al., 1967] and heating rate. Despite the wealth of published works on the dehydroxylation of kaolinite, there is no general consensus over the kinetics and mechanism of the entire reaction.

The calcination of such clay could be accomplished either by flash calcination or soak calcination. Flash calcination is achieved by rapid heating ($\approx$ several tenths of seconds) followed by rapid cooling of the powdered clay material suspended in gas; whereas soak calcination is achieved by slow heating for relatively long periods. According to the literature [Salvador, 1995], flash-calcined products have shown peculiar structural properties and reactivity that makes them a potential clinker substitute. Thus, a good knowledge on the nature, composition and methods of calcining the clay material are crucial to obtain a highly reactive pozzolanic product. For instance, the crystallinity, the amount of metakaolinite and the particle size of the calcined clay strongly affects its performance as SCM.

2.3.2 Kinetics of dehydroxylation

Dehydroxylation of kaolinite is accompanied by the loss of chemically bonded hydroxyls and consequently, a structural disorder in the kaolinite framework causes the formation of amorphous phase, namely metakaolinite. This phenomenon is revealed by the appearance of an endothermic peak between temperatures 800-1000 K. Analysis of the differential thermal patterns of this peak is a common way of studying the reaction kinetics of the clay material. Thermal analysis on the dehydroxylation of kaolinite has been studied by using different techniques to examine the value of kinetic parameters, specifically the activation energy (E) and the frequency factor (A).

Generally kinetic parameters for solid state reactions have been studied either by model-fitting or model-free (isoconversional) methods. Model fitting methods yield single value of activation energy which cannot account for the variation of activation energy due to the complexity of the solid state reaction. The values obtained by these methods are averages that do not reflect changes in the kinetics and mechanism with the temperature and the extent of conversion. Whereas, model-free methods allow kinetic predictions to be accomplished as a function of the extent of reaction. As such, the kinetic analysis is carried out over a set of kinetic runs and gives better estimation of kinetic parameters. Both methods have been practiced to determine the kinetic parameters of kaolinite dehydroxylation. None of them is free of flaws, but model free methods got an upper hand.

The use of empirical models (model-fitting methods) to study the dehydroxylation of kaolinite has been carried out to examine the kinetics and reaction mechanism of the dehydroxylation reaction [Brindley et al., 1967; Dion et al., 1998; Murray and White, 1955; Sharp et al., 1966]. Most of these studies attempt to solve if the reaction mechanism follows first order or diffusion controlled mechanism, which has been a dispute over the years. Yet, dehydroxylation of kaolinte remains controversial, where some authors suggest the reaction obeys a first-order kinetic law [Allison, 1955; Dion et al., 1998; Murray and White, 1955] whereas others suggest a diffusion model [Criado et al., 1984; Horvath, 1985; Redfern S., 1987].

Kinetic parameters based on isoconversional methods are usually obtained using thermogravimetric experiments. Among these methods, Kissinger's method is one of the most popular methods to calculate kinetic parameters for dehydroxylation of kaolinite clays [Kissinger, 1956]. Accordingly, when a reaction occurs in differential thermal analysis, the thermal properties of the sample vary with heating rate and this variation is manifested by deflection of temperature peaks. Analyzing the shift in peak temperature at different heating rates during thermogravimetric experiment is the core concept to

determine the kinetic parameters. A complete derivation of the method can be referred elsewhere in the literature [Chen et al., 1993; Kissinger, 1957, 1956; Llópiz et al., 1995].

Although the kinetics of kaolinite dehydroxylation has been broadly studied, there is no single activation energy and frequency factor that characterize the dehydroxylation process. Table 2.2 provides a summary of kinetic parameters of kaolinite dehydroxylation from literature. The reason behind the diversity of values could be due to their dependence on the natural composition, crystallinity and particle size distribution of the kaolinite sample. The fact that dehydroxylation of kaolinite is a complex process involving many individual steps, has been demonstrated by the dependence of activation energy on the extent of conversion [Ortega et al., 2010].

TABLE 2.2: A summary of kinetic parameters of kaolinite dehydroxylation from literature

E(kJ/mol)	A(s^{-1})	Method	Source	Reference
177	4.57×10^8	Thermogravimetry	Florida,USA	Kissinger [1956]
162	1.26×10^7	Thermogravimetry	Georgia,USA	Kissinger [1956]
242	2.21×10^8	Effluent gas analysis	Rep.Czech	Ptáček et al. [2010]
196	9.6×10^8	TGA	India	Saikia et al. [2002]
195	8.58×10^{14}	DTG	Rep.Czech	Ptáček et al. [2011]
193	1.70×10^7	DTA	USA	Bellotto et al. [1995]
163	2×10^{12}	DTA	USA	Levy and Hurst [1993]

2.4 Modeling thermal calcination of kaolinite

Today the use of computational modeling to tackle complex engineering problems in the quest for optimal solutions in many fields of studies is a common practice. Hence, mathematical models have been used to harvest any process related characteristics for the calcination of kaolinite such as dehydroxylation mechanism, conversion and phase transformation.

There has been little effort to understand calcination of kaolinite clays through modeling. Indeed significant advances have been made in modeling fluid-solid, mainly gas-solid reactions [Bhatia, 1985; Georgakis et al., 1979; Patisson et al., 1998; Szekely and Propster, 1975; Wen and Wang, 1970]. Most of them are based on grain model and shrinking core models to study the heat and mass transfer during reactions that involve gas-solid interactions. However, these models consider several assumptions. Among them are steady state and pseudo steady state approximations that ignore the accumulation term in the gaseous phase [Bhatia, 1985; Szekely and Propster, 1975]. Such assumptions are mainly

made to simplify and circumvent mathematical difficulties; and are not recommended in transient phenomena [Wen and Wang, 1970]. The isothermal assumptions rendered in most grain and shrinking core models is another drawback of such models [Georgakis et al., 1979]. When most of gas-solid reactions involve exothermic and endothermic reactions, it may impose temperature variation affecting the internal and external heat transfer in the grain, thus, isothermal assumptions may only be used for a known cases [Patisson et al., 1998].

In an attempt to study flash calcination of kaolinite clay, Salvador and Davies [1994] presented a simplified thermochemical model which is used to examine the behavior of kaolinite particles that are plunged into a hot gas atmosphere. In this model, different particle sizes were investigated for their calcination behavior at different gas temperatures (823–1273 K). The model predicts fast conversion rates at higher temperatures (1273 K). For instance, 100 µm particles are observed to dehydroxylate in 0.1 seconds. The fast heating rate observed during flash calcination causes rapid generation of vapor and is suggested to be the reason for particle decrepitation observed during flash dehydroxylation of kaolinite [Bridson et al., 1985]. However, this model does not consider the effect of intra-particle processes that could influence dehydroxylation process. Favergeon et al. [2013] also presented a kinetic model for kaolinite dehydroxylation at grain scale that could be applied for heat and mass transfers at reactor scale. The kinetic model is entirely based on the dehydroxylation reaction as a rate limiting reaction where several built-in empirical models are used to monitor dehydroxylation reaction. The model is able to predict the dependence of dehydroxyalation rate on calcination temperature and vapor pressure. Moreover, the kinetic rate is found to be significantly affected by the powder height in the reactor. This model is based on complex variables such as areic frequency of nucleation, areic reactivity of growth, vapor pressure and so on that require to apply several assumptions.

The above mentioned models by [Salvador and Davies, 1994] and [Favergeon et al., 2013], however, have some limitations when addressing the complex behavior of kaolinite clay calcination at different process conditions. For instance, none of them predicts the composition of the calcined material and the phase transformation of kaolinite particle when the temperature exceeds 1273 K.

On the other hand, modeling the calcination of limestone particles has been extensively studied. Many of the investigations have been done on the calcination and simultaneous sintering processes of limestone particles with the aid of mathematical models. Borgwardt [Borgwardt, 1985] found that the calcination reaction was kinetically controlled except for the final stage of reaction where the diffusion of CO_2 through the product layer was rate limiting. Silcox et al. [Silcox et al., 1989] also developed a calcination model

of limestone ($CaCO_3$) and ($Ca(OH)_2$) particles where the decomposition of the parent material at the reactant–product interface was described by a shrinking core model by solving kinetic and transport equations for the gas and solid species. The model reliably predicts the effects of particle size, temperature, time and relative rates of surface area development. The study concluded that the escape of CO_2 does not significantly slow down the calcination reaction rate for small particles, and thus smaller lime particles produce more reactive CaO particles in shorter period and at lower temperatures. But, the hydrate particle produces more reactive CaO than do carbonates. This implies rapid calcination rate for the hydrates, $Ca(OH)_2$ than carbonates, $CaCO_3$.

The model developed by Hu and Scaroni [Hu and Scaroni, 1996] considers the heat and mass transfer and chemical kinetics for calcination of pulverized limestone particles under furnace injection conditions. The model show a significant influence of heat transfer, mass transfer and chemical kinetics on the calcination rate of limestone. Moreover, due to location-dependent calcination process, a gradient in temperature and CO_2 partial pressures are observed. Under such conditions, the calcination of smaller limestone particles ($\approx 63\mu$m) is observed in less than 0.2 seconds at 1473 K furnace temperature.

Takkinen et al. [2012] also investigated the heat and mass transfer phenomena during calcination of limestone through modeling. Two modeling approaches were used, namely the shrinking core model and a transient numerical particle model where the mass, momentum and energy equations are solved during calcination. The numerical particle model depicts faster and uniform conversion for smaller particles at different calcination stages. Furthermore, high temperature is observed to decrease the reaction time. Over all, the importance of advection in the intraparticle transport during calcination was highlighted for the numerical particle model. In their study the applicability of shrinking core models towards lime calcination is compared with the numerical particle model. Both models show certain degree of differences in their output, the difference being significant for small particle sizes and higher CO_2 concentrations in the surrounding gas. These differences are however modest when the model assumes an apparent reaction rate than infinite reaction rate.

Other calcination studies on limestone has also been demonstrated for the purpose of cement production either at the precalciner or at the rotary kiln [Fidaros et al., 2007; Mikulčić et al., 2012]. Their investigation focuses on the impact of partial pressure, particle size distribution and porosity on the degrees of conversion. Alike the above studies, the influence of temperature, particle size and partial pressure of CO_2 on the calcination process has been reported.

The usefulness of such limestone models in this study is the similarity of the calcination process and thus, the modeling approach is somehow similar. However, the effect of

process variables during calcination of limestone is quite different from that of kaolinite. i.e., the product of limestone calcination which is CaO may not further transform into a different phase that affect the performance of cement. Hence, the severe calcination condition and long residence time at the kiln system might have little effect on final property of lime, if not on the cost of production. The exothermic nature of some reactions involved during kaolinite rich clay calcination, however, makes the temperature control more crucial and also more difficult, in order to obtain the optimum calcines.

2.5 Experimental study on flash calcination of kaolinite

Flash calcination of kaolinite has been investigated by several authors [Bridson et al., 1985; Meinhold et al., 1992; Meinhold and Salvador, 1994; Slade and Davies, 1991; Slade et al., 1991, 1992]. In most cases the powdered kaolinite clay is exposed to high temperature($\approx$ 1273K) for short period of time, usually 0.5 to 1 second. Any change in characteristics of the calcines is examined by rapid cooling at various stages during calcination. Thus, flash calcined kaolinites undergo structural changes such as internal voids. These changes are due to rapid generation of vapor, especially for residence times beyond 0.3 seconds [Slade and Davies, 1991]. The flash calcines also display lower density than the original kaoilinite sample [Bridson et al., 1985]. However, as the residence time inside the calciner increases, the specific gravity progressively increases.

Flash calcination tests are also studied using different laboratory scale and pilot scale flash calciners to examine the mechanism of dehydroxylation reaction [Meinhold and Salvador, 1994]. These tests are carried out at different temperature and residence time. In all cases, the rate of flash dehydroxylaton is influenced by diffusion of vapor and the process is represented by 3 dimensional diffusion model. However, a change in mechanism is observed at higher degrees of dehydroxylation. The different activation energies calculated for the calcines produced by the different flash calciners may be explicable due to the impact of vapor pressure inside the calciner that change the gas flow characteristics, and also due to different sample introduction methods for each calciner.

In a comparative study of calcined kaolinite particles from an industrial flash calciner and conventional rotary kiln calciner, the chemical composition of the calcined metakaolinite product is not influenced by the method of calcination [San Nicolas et al., 2013]; rather the physical property of calcines is affected significantly. Since the calcination process in rotary kiln calciner is achieved at low temperatures 920–973 K for about 3–5 hours, agglomeration of the calcined product is observed. In an industrial flash calciner, the process is accomplished in few tenths of seconds at temperatures 1273–1473 K. The

flash calcines display spherical morphology compared to the conventional kiln products, furthermore, the flash calcines show high proportion of mullite due to direct contact between the flame and clay particles inside the calciner.

Chapter 3

Single particle calcination model

This chapter describes the numerical effort used to model the calcination of kaolinite rich clay particles. It briefly discusses the set of governing equations that characterize the energy and fluid flow during calcination along with boundary conditions and method of discretization used to solve the equations. It also gives an overview of the modeling tools used in this study.

3.1 Fundamentals of CFD

Computational Fluid Dynamics (CFD) involves the analysis of a set of partial differential equations that characterize the flow of a fluid. For instance, consider the general transport equation which is given as:

$$\frac{\partial(\rho\psi)}{\partial t} + \nabla \cdot (\rho \mathbf{U}\psi) = \nabla \cdot (D\nabla\psi) + S_\psi \tag{3.1}$$

The above equation represents the flow and transport of fluids in which first two terms in the left side of the equation correspond to the transient and convective terms, respectively. The right side equations correspond to the diffusion and source terms, respectively. Where ψ is a dependent variable transported due to the existence of a velocity field, $\mathbf{U}$ and the gradient of the property transported, $\nabla\psi$. The source term, S_ψ accounts for any sources or sinks that either create or destroy ψ.

A common CFD practice involves the discretization of the computational domain into a number of cells or control volumes. The equation is then integrated over the control volume so as to discretize the partial differential equations to algebraic equations by using finite volume method. The set of algebraic equations are solved to calculate the values at cell centers, after the initial and the boundary conditions of the problem are

specified properly. In this way CFD provides an approximation to the analytical solution of the general governing equations.

3.2 Description of the clay particle calcination model

The problem under investigation may be understood in such a way that when a kaolinite clay particle initially at room temperature is exposed to a hot environment, different physical and chemical processes may take place. Among them are heat transfer from the surrounding, evaporation of any available moisture, dehydroxylation and transformation of kaolinite into different phases sequentially. In order to substantiate the entire process numerically, a particle model is developed.

In practice, the shape of such clay particles may be better represented by flat sheet (flake-like). Due to the lack of accurate description of particle shape, the clay particles are assumed as spheres, as most commonly used in particle shape approximation (e.g., pulverized coal particles), and an one-dimensional (1D) spherical particle model is developed to simulate thermal calcination of these particles. Figure 3.1 illustrates the 1D calcination model showing the interaction of the clay particle with its surrounding. As shown in the figure, the exchange of mass and heat with the surrounding gas is accomplished by radiation and convection through a gas film surrounding the particle, where the temperature, mass concentration and other physical properties in the gas film are evaluated using a simple $1/3^{rd}$ rule [Abramzon and Sirignano, 1989].

As heating continues, the kaolinite clay particle conversion proceeds by releasing free water and crystal water out of the particle to yield the amorphous material called metakaolinite. When the particle temperature reaches certain level beyond complete dehydroxylation, phase transformation of metakaolinite commences. Depending on the process conditions, the particle conversion and transformation of the clay product is examined based on the series of reactions given in section 2.3.1, reactions (2.1)–(2.5). The sequence of reactions is governed by the temperature and kinetic parameters at each reaction step; as such, high temperature and fast reaction rates may increase the speed of phase transformation into unnecessary products such as mullite. Therefore, the kinetic parameters for each reaction need to be carefully picked from literature or experimentally determined.

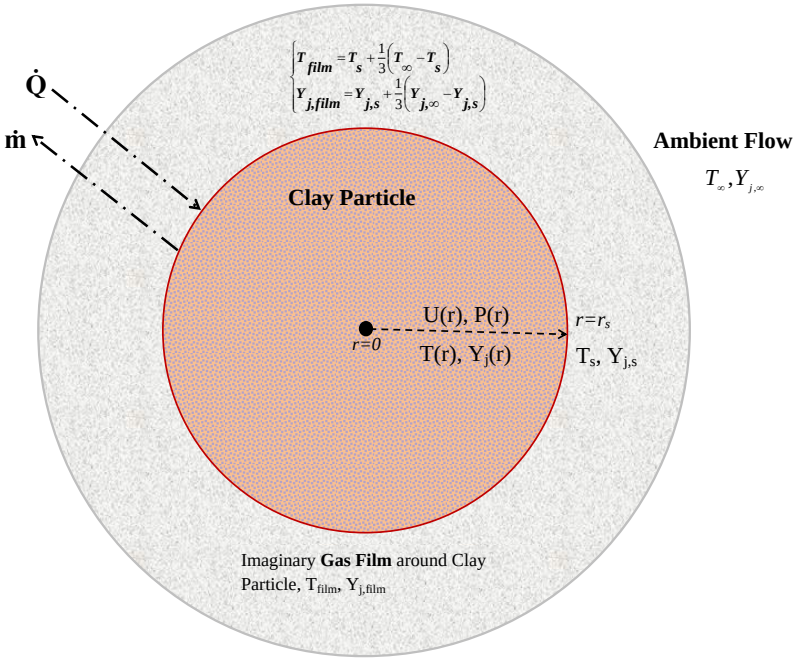

FIGURE 3.1: A sketch of 1D clay particle calcination model

3.2.1 Main assumptions

The main assumptions used in the model development are:

- The clay particle is spherical in shape and homogeneous in composition,
- 1D profile, i.e., the dominant variations in key parameters occur in the radial direction (from the particle center to particle surface)
- Local thermal equilibrium exist within the clay particle, i.e., different phases at the same temperature locally.
- Possible shape changes due to swelling or shrinking of the particle are neglected,
- The porosity of kaolinite particle hardly changes up on thermal treatment unless it undergoes sintering beyond 1373 K [Chen et al., 2003]. Hence, constant particle porosity is assumed,
- The heat and mass transfer conditions at the particle surface are symmetrical,
- Gas species and the gas mixtures follow the equation of state for an ideal gas,
- The same value of effective diffusivity (D_{eff}) has been assumed for all the gaseous species, such assumption has been commonly used in literature [Lu et al., 2008; Takkinen et al., 2012].

3.2.2 Governing equations

Like any modeling process, numerical study of kaolinite calcination begins with a physical model that is described by a set of PDEs which are developed based on conservation laws of physics. The general governing equations that characterize the thermal conversion of kaolinite during calcination are summarized as follows:

$$\frac{\partial(\varepsilon\rho_g)}{\partial t} + \mathrm{div}(\varepsilon\rho_g \mathbf{U}) = S_g \tag{3.2}$$

$$\mathbf{U} = -\frac{\eta}{\mu}\nabla P \tag{3.3}$$

$$\frac{\partial(\varepsilon\rho_g Y_j)}{\partial t} + \mathrm{div}(\varepsilon\rho_g \mathbf{U} Y_j) = \mathrm{div}(\varepsilon\rho_g D_{eff}\nabla Y_j) + S_{Y_j} \tag{3.4}$$

$$\frac{\partial}{\partial t}\Big(\sum_i \rho_i h_i + \varepsilon\rho_g h + \rho_{fw} h_{fw}\Big) + \mathrm{div}(\varepsilon\rho_g \mathbf{U} h) = \mathrm{div}(k_{eff}\nabla T) + \mathrm{div}\Big(\sum_j h_j \varepsilon\rho_g D_{eff}\nabla Y_j\Big) + S_h \tag{3.5}$$

$$\frac{\partial(\rho_{s,i} Y_{s,i})}{\partial t} = S_{y,i} \tag{3.6}$$

In the above equations, Eq. 3.2–3.4 represent the continuity equation, momentum equation modified with Darcy's law in a porous medium, and the species transport equations for the gaseous phases, respectively. Eq. 3.5 is a combined energy equation where the influence of gases, solids and moisture on the transfer of energy is incorporated. The last equation represented in Eq. 3.6 is the continuity equation for solid species.

The rate expression and kinetic parameters for the reactions involved during calcination of kaolinite clay are represented as shown in Table 3.1.

TABLE 3.1: The expression of reaction rate and kinetic parameters used in the model

Reaction	Rate expression	A (s^{-1})	E (kJ/mol)	△H (kJ/kg)	Reference
2.1	$\dot{r}_1 = \frac{\partial \rho_{\mathrm{fw}}}{\partial t} = k_1 \rho_{fw}$	5.13×10^{10}	88	-2242	[Bryden and Hagge, 2003]
2.2	$\dot{r}_2 = \partial\rho_{kl}/\partial t = k_2 \rho_{kl}$	6.3×10^{9}	180	-632	(A,E):this work, △H: [Weber and Roy, 1965]
2.3	$\dot{r}_3 = \frac{\partial}{\partial t}(\rho_{mk}) = k_3 \rho_{mk}$	1.7×10^{16}	405	230	[Gerardin and Sundaresan, 1994]
2.4	$\dot{r}_4 = \frac{\partial \rho_{sp}}{\partial t} = k_4 \rho_{sp}$	9.1×10^{15}	424	84	(A,E): [Ptáček et al., 2012], △H: [Holm, 2001]
2.5	$\dot{r}_5 = \frac{\partial \rho_{sil}}{\partial t} = k_5 \rho_{sil}$	1.75×10^{10}	274	42	(A,E): [Ptáček et al., 2012], △H: [Holm et al., 1967]

The expression of key physical and transport properties used in the above governing equations are summarized in Table 3.2.

TABLE 3.2: The Physical and transport properties and their expression in the model

Property	Value/Expression	Reference
Sensible enthalpy of gas mixture, h	$\sum_j Y_j h_j$	
Sensible enthalpy of species, h_j	$\int_{T_{ref}}^{T} C_{p,j}(T)dT$	
Rate constant of k^{th} reaction, k_k	$A_k exp(-E_k/RT)$	
Effective conductivity, k_{eff}	$\varepsilon k_g + (1-\varepsilon)k_s$	[Takkinen et al., 2012; Tavman, 1996]
Conductivity of solid, k_s	0.3	[Michot et al., 2008]
Effective diffusivity, D_{eff}	$\frac{\varepsilon}{\tau}\left(\frac{1}{D_{AB}}+\frac{1}{D_k}\right)^{-1}$	[Benitez, 2009; Silcox et al., 1989]
Molecular diffusivity, D_{AB}	$-2.775 \times 10^{-6} + 4.479 \times 10^{-8}T + 1.656 \times 10^{-10}T^2$	[Bolz and Tuve, 1976]
Knudsen diffusivity, D_k	$48.50 d_p \sqrt{\frac{T}{MW_g}}$	[Benitez, 2009; Silcox et al., 1989]
Pore size, d_p	0.3×10^{-6}	[Diamond, 1970]
Permeability, η	1×10^{-12}	[Reinecke and Sleep, 2002]
Particle emissivity, ω	0.7	[Bergman et al., 2011]
Tortuosity, τ	1.5	this work

The expression of the source/sink terms that appear in the above set of governing equations is based on the rate expression given in Table 3.1. Since evaporation and dehydroxylation are the only reactions that generate gaseous species; the source/sink terms that appear in the continuity equation, S_g and in the transport equation, S_{Y_j} are basically equivalent. The contribution of other gases (O_2 and N_2) during reaction is is negligible. The source/sink term appearing in the energy equation is the heat effects summed over all the five reactions. The expression of all source/sink terms are summarized as follows;

$$\begin{aligned} S_g = S_{Y_j} &= \dot{r}_1 + \dot{r}_2 \frac{2MW_{H_2O}}{MW_{kl}} \\ S_h &= \sum_{k=1}^{k=5} \dot{r}_k \triangle H_k \end{aligned} \tag{3.7}$$

The source term expression for solid species, S_{Y_i} is based on the rate of conversion of individual species during calcination reaction and is summarized in Table 3.3.

Temperature dependent heat capacity of solid species is used in the study [Knovel, 2013; Robie et al., 1979]. The heat capacity values for each solid components is summarized in Table 3.4.

TABLE 3.3: The expressions for solid species source/sink terms during calcination of kaolinite clays

Source(sink) term	Expression
For kaolinite, S_{kl}	$-\dot{r}_2$
For metakaolinite, S_{mk}	$\dot{r}_2(\mathrm{MW_{mk}}/\mathrm{MW_{kl}}) - \dot{r}_3$
For spinel, S_{sp}	$\dot{r}_3(\mathrm{MW_{sp}}/2\mathrm{MW_{mk}}) - \dot{r}_4$
For mullite, S_{mu}	$\dot{r}_4(2\mathrm{MW_{mu}}/3\mathrm{MW_{sp}})$
For silica, S_{sil}	$\dot{r}_3(\mathrm{MW_{sil}}/2\mathrm{MW_{mk}}) + \dot{r}_4(5\mathrm{MW_{sil}}/3\mathrm{MW_{sp}}) - \dot{r}_5$
For cristobalite, S_{cr}	$\dot{r}_5(\mathrm{MW_{sl}}/\mathrm{MW_{cr}})$

TABLE 3.4: Temperature dependent heat capacity of solid species

Heat capacity	Value (J/(kg·K))
$C_{p,kl}$	$(200.58 - 0.795T + 4.42 \times 10^{-3}T^2 - 8.25 \times 10^{-6}T^3 + 7.65 \times 10^{-9}T^4 - 3.55 \times 10^{-12}T^5 + 6.55 \times 10^{-16}T^6)1000/MW_{kl}$
$C_{p,mk}$	$(146.5 - 0.51T + 2.98 \times 10^{-3}T^2 - 5.68 \times 10^{-6}T^3 + 5.29 \times 10^{-9}T^4 - 2.45 \times 10^{-12}T^5 + 4.48 \times 10^{-16}T^6)1000/MW_{mk}$
$C^{\dagger}_{p,sp}$	$(146.5 - 0.51T + 2.98 \times 10^{-3}T^2 - 5.68 \times 10^{-6}T^3 + 5.29 \times 10^{-9}T^4 - 2.45 \times 10^{-12}T^5 + 4.48 \times 10^{-16}T^6)1000/MW_{sp}$
$C_{p,mu}$	$(7.55 \times 10^2 - 2.94 \times 10^{-2}T - 6.58 \times 10^3 T^{-0.5} + 3.45 \times 10^{-6}T^{-2})1000/MW_{mu}$
$C_{p,sil}$	$(21.27 + 0.12T - 1.99 \times 10^{-4}T^2 + 2.29 \times 10^{-7}T^3 - 1.72 \times 10^{-10}T^4 + 7.295 \times 10^{-14}T^5 - 1.29 \times 10^{-17}T^6)1000/MW_{sil}$
$C_{p,cr}$	$(72.753T + 1.3 \times 10^{-3}T + 4.13 \times 10^6 T^{-2})1000/MW_{cr}$

† The heat capacity of spinel-type phase is not available in the literature. Thus, it is assumed to have similar heat capacity as that of metakaolinite.

3.2.3 Boundary conditions

Boundary conditions at the particle center (at $r = 0$) are determined by symmetry as:

$$\left.\frac{\partial T}{\partial t}\right|_{r=0} = 0; \qquad \left.\frac{\partial Y_j}{\partial t}\right|_{r=0} = 0; \qquad \left.\frac{\partial P}{\partial t}\right|_{r=0} = 0 \tag{3.8}$$

At the surface of the particle ($r = R_P$), the exchange of mass and heat with the surrounding gas film is driven by the external convective mass transfer coefficient, h_m and convective heat transfer coefficient, h_T, respectively; which in turn is calculated from the empirical correlations available in the literature [Ranz and Marshall, 1952]. The Stefan flow effect is not taken into account in this work, mainly due to the comparatively small amount of water vapor flow released during clay calcination process. Thus, the boundary conditions at the particle surface are:

$$
\begin{aligned}
k_{eff}\frac{\partial T}{\partial t}\bigg|_{r=R_p} &= h_T(T_\infty - T_s) + \omega\sigma(T_{rad}^4 - T_s^4) \\
Nu = \frac{h_T D_p}{k_g} &= 2 + 0.64(Re)^{\frac{1}{2}}(Pr)^{\frac{1}{3}} \\
D_{j,m}\frac{\partial Y_j}{\partial t}\bigg|_{r=R_p} &= h_m(Y_{j,\infty} - Y_{j,s}) \\
Sh = \frac{h_m D_p}{D_{AB}} &= 2 + 0.64(Re)^{\frac{1}{2}}(Sc)^{\frac{1}{3}} \\
P|_{r=R_p} &= P_{atm}
\end{aligned}
\tag{3.9}
$$

The physical properties in the gas film around the particle are evaluated based on the reference conditions that can be calculated by a simple $1/3^{rd}$ rule [Abramzon and Sirignano, 1989], from which the non-dimensional constants such as Nu, Pr, Re, Sc, and Sh numbers are computed. Thus, the reference conditions in temperature and mass fraction at the gas film are calculated as,

$$
\begin{aligned}
T_{film} &= T_s + \frac{1}{3}\Big(T_\infty - T_s\Big) \\
Y_{j,film} &= Y_{j,s} + \frac{1}{3}\Big(Y_{j,\infty} - Y_{j,s}\Big)
\end{aligned}
\tag{3.10}
$$

3.2.4 Initial conditions

Apart from boundary conditions, the transient calcination model require well defined initial conditions where initial values of flow variables are specified in the flow domain. These conditions usually describe the states of the solid and gas phases at the beginning of the process (t = 0).
The initial conditions acquired are:

$$
\begin{aligned}
&T|_{t=0} = 298.15K; \qquad P|_{t=0} = P_{atm} \\
&Y_{\mathrm{H_2O}}\big|_{t=0} = 0; \quad Y_{\mathrm{O_2}}\big|_{t=0} = 0.23; \quad Y_{\mathrm{N_2}}\big|_{t=0} = 0.77
\end{aligned}
\tag{3.11}
$$

3.3 Discretization

Discretization of the calculation domain is achieved by systematically dividing the space and dependent variables so that the governing differential equations could be expressed with simple algebraic equations that can be solved easily. The discretization of the governing equations in the present work is based on finite volume method (FVM), which is one of the well studied schemes [Patankar, 1980; Versteeg and Malalasekera, 2007].

The discretized equations are then assembled to a standard form that can be solved by using TDMA (Tri-Diagonal Matrix Algorithm).

$$a_P\psi_P = a_W\psi_W + a_E\psi_E + S_u \tag{3.12}$$

where ψ is a property that can be computed, for example the temperature, mass fraction, pressure and so on. The subscripts P, W and E denote the position at current cell-center, at the west and the east neighboring cell-centers, respectively. S_u is the source term, if any.

Since the transient particle model output is a function of time and position, the discretization is carried out for both of the domains. Thus, numerical discretization of such time-dependent partial differential equations (PDE) need to be fully discretized in both time and space. The governing equations are discretized in space first to transform PDEs into ordinary differential equations (ODEs), followed by time integration of ODEs to advance in time.

3.3.1 Spatial discretization

The discretization of the single particle model is accomplished by dividing it into a finite number of control volumes (CV). In order to integrate the PDE's over each cell, the basic mesh is defined by a set of points (nodes) from the domain so that to each node a control volume is assigned. The computational domain in this work is shown in Figure 3.2, where the spherical particle is divided into N equidistant nodes, $\triangle r$. To simplify the notation in accordance with the standard notation widely used in many of the CFD books, the letters P, W and E denote the nodes at r_i, $r_i - 1$ and $r_i + 1$, respectively. At these nodes, the scalar variables such as the temperature, pressure, density and mass fraction are evaluated. Each control volume is bounded by faces that are located midway between the grid points. These faces are represented by w and e which are located at $r_i - \frac{1}{2}\triangle r$ and $r_i + \frac{1}{2}\triangle r$, respectively. At these faces, velocity components are calculated. In this study, discretization is based based on the upwind scheme for the convection term, and the central difference scheme for the diffusion term.

3.3.2 Temporal discretization

Temporal discretization has been carried out using fully implicit method. The advantage of this method is its unconditional boundedness and robustness for any size of time step [Patankar, 1980; Versteeg and Malalasekera, 2007]. Hence, the governing equations are

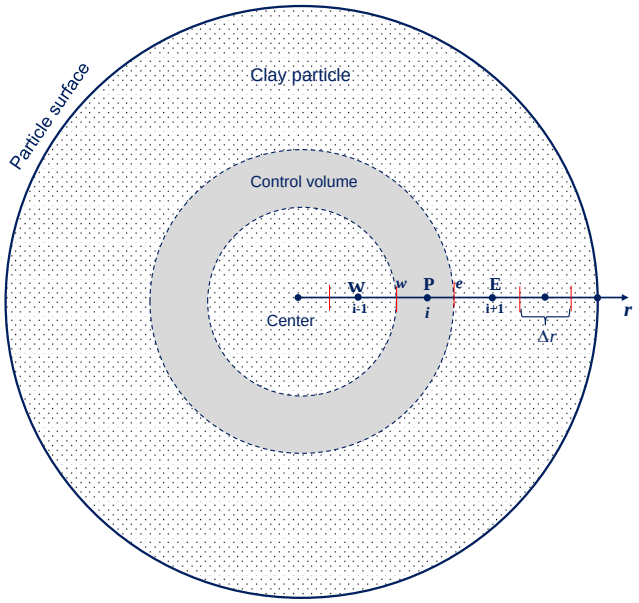

FIGURE 3.2: Discretization of the one dimensional clay particle

temporally discretized over a time step ($\triangle t$). A general expression for the transient term in the PDEs during time marching of a scalar variable ϕ is given as;

$$\frac{\partial \psi}{\partial t} = F(\psi) \tag{3.13}$$

where F is anonymous function that may have any spatial discretization. The first-order accurate implicit temporal discretization is given by ;

$$\frac{\psi - \psi^o}{\triangle t} = F(\psi) \tag{3.14}$$

where the variable with superscript, ψ^o denotes the value of the quantity at the previous time, $t - \triangle t$, while the values of ψ are evaluated at current time, t. This way, the fully implicit scheme is implemented to all transient governing equations.

3.3.3 Final discretized equations

As briefly discussed in the previous section, the final form of the energy, transport and continuity equations are discretized and rearranged into a standard form $a_P\psi_P = a_W\psi_W + a_E\psi_E + S_u$. The final solution is summarized by sorting the value of the coefficients. Solving the discretized energy equation by using TDMA solver gives the value of temperature. The value of coefficients for the discretized energy equation are summarized in Table 3.5.

TABLE 3.5: A solution to the discretized energy equation

Coefficient	Solution of energy equation
$\mathbf{a_W}$ (cell center)	0.0
$\mathbf{a_W}$ (internal cells)	$\left(\frac{k_{eff}A}{\triangle r}\right)_w + \left(\frac{\varepsilon\rho_g C_{p,g}\mathbf{U}A}{2}\right)_w$
$\mathbf{a_W}$(cell surface)	$\left(\frac{k_{eff}A}{\triangle r}\right)_w + \left(\frac{\varepsilon\rho_g C_{p,g}\mathbf{U}A}{2}\right)_w$
$\mathbf{a_E}$ (cell center)	$\left(\frac{k_{eff}A}{\triangle r}\right)_e$ - $\left(\frac{\varepsilon\rho_g C_{p,g}\mathbf{U}A}{2}\right)_e$
$\mathbf{a_E}$ (internal cells)	$\left(\frac{k_{eff}A}{\triangle r}\right)_e$ - $\left(\frac{\varepsilon\rho_g C_{p,g}\mathbf{U}A}{2}\right)_e$
$\mathbf{a_E}$ (cell surface)	0.0
$\mathbf{a_P}$ (cell center)	$\frac{\rho C_p\triangle V}{\triangle t} + \mathbf{a_E} + \mathbf{a_W} + (\varepsilon\rho_g C_{p,g}\mathbf{U}A)_e$ - $(\varepsilon\rho_g C_{p,g}\mathbf{U}A)_w$
$\mathbf{a_P}$ (internal cells)	$\frac{\rho C_p\triangle V}{\triangle t} + \mathbf{a_E} + \mathbf{a_W} + (\varepsilon\rho_g C_{p,g}\mathbf{U}A)_e$ - $(\varepsilon\rho_g C_{p,g}\mathbf{U}A)_w$
$\mathbf{a_P}$ (cell surface)	$\frac{\rho C_p\triangle V}{\triangle t} + \mathbf{a_E} + \mathbf{a_W} + (\varepsilon\rho_g C_{p,g}\mathbf{U}A)_e - (\varepsilon\rho_g C_{p,g}\mathbf{U}A)_w + A_{surf}h_T + 4A_{surf}\omega\sigma(T_P^o)^3$
$\mathbf{S_u}$ (cell center)	$\frac{(\rho C_p)^o T_p^o\triangle V}{\triangle t} + \sum_{k=1}^{5}\dot{r}_k\triangle H_k\triangle V$
$\mathbf{S_u}$ (internal cells)	$\frac{(\rho C_p)^o T_p^o\triangle V}{\triangle t} + \sum_{k=1}^{5}\dot{r}_k\triangle H_k\triangle V$
$\mathbf{S_u}$ (cell surface)	$\frac{(\rho C_p)^o T_p^o\triangle V}{\triangle t} + \sum_{k=1}^{5}\dot{r}_k\triangle H_k\triangle V + A_{surf}h_T T_\infty + A_{surf}\omega\sigma(T_{rad}^4 + 3(T_P^o)^4)$

- The superscript, ^{o}, indicates the value of the parameter at the previous time step
- $\rho C_p = \sum_i \rho_i C_{p,i} + \sum_j \varepsilon\rho_g Y_j C_{p,j} + \rho_{fw} C_{p,fw}$

At the outer most control volume, the final discretized energy equation need to address the heat source term S_h at the particle surface due to convection and radiation. Thus, the heat source term S_h is integrated at the control volume to yield:

$$\int_{\triangle t}\int_{cv} S_h dV dt = h_T A_{surf}(T_\infty - T_s) + A_{surf}\omega\sigma(T_{rad}^4 - T_s^4) \tag{3.15}$$

The nonlinear radiation source term is handled as described elsewhere in the literature [Yin et al., 2010], where the linearized radiation term will have the form,

$$A_{surf}\omega\sigma(T_{rad}^4 - T_s^4) \approx A_{surf}\omega\sigma\Big(T_{rad}^4 - (T_P^o)^4 - 4(T_P^o)^3(T_P - T_P^o)\Big) \tag{3.16}$$

Discretizing and integrating the transport equation solves for the mass fraction of gas species, Y_j. The solution of the transport equation sorted in accordance with the standard form of notation is summarized in Table 3.6.

Solving the continuity equation requires substituting the physical velocity at the east and west interfaces using Darcy's flow equation Eq. 3.3. The solution of the resulting discretized equation solves for the pressure correction term, P′ as shown in Table 3.7.

The velocity at the outer most control volume is derived from the discretized continuity equation as;

$$\mathbf{U}_e = \Big[\frac{S_g\triangle V}{\varepsilon} - \frac{(\rho_g - \rho_g^o)\triangle V}{\triangle t} + (\rho_g\mathbf{U}A)_w\Big]/(\rho_g A)_e \tag{3.17}$$

TABLE 3.6: A solution to the discretized transport equation of gases

Coefficient	Solution of transport equation
$\mathbf{a_W}$ (cell center)	0.0
$\mathbf{a_W}$ (internal cell)	$\left(\frac{\varepsilon\rho_g D_{eff} A}{\triangle r}\right)_w + \left(\frac{\varepsilon\rho_g \mathbf{U} A}{2}\right)_w$
$\mathbf{a_W}$ (cell surface)	$\left(\frac{\varepsilon\rho_g D_{eff} A}{\triangle r}\right)_w + \left(\frac{\varepsilon\rho_g \mathbf{U} A}{2}\right)_w$
$\mathbf{a_E}$ (cell center)	$\left(\frac{\varepsilon\rho_g D_{eff} A}{\triangle r}\right)_e - \left(\frac{\varepsilon\rho_g \mathbf{U} A}{2}\right)_e$
$\mathbf{a_E}$ (internal cells)	$\left(\frac{\varepsilon\rho_g D_{eff} A}{\triangle r}\right)_e - \left(\frac{\varepsilon\rho_g \mathbf{U} A}{2}\right)_e$
$\mathbf{a_E}$ (cell surface)	0.0
$\mathbf{a_P}$ (cell center)	$\frac{\varepsilon\rho_g \triangle V}{\triangle t} + \mathbf{a_E} + \mathbf{a_W} + (\varepsilon\rho_g \mathbf{U} A)_e - (\varepsilon\rho_g \mathbf{U} A)_w$
$\mathbf{a_P}$ (internal cells)	$\frac{\varepsilon\rho_g \triangle V}{\triangle t} + \mathbf{a_E} + \mathbf{a_W} + (\varepsilon\rho_g \mathbf{U} A)_e - (\varepsilon\rho_g \mathbf{U} A)_w$
$\mathbf{a_P}$ (cell surface)	$\frac{\varepsilon\rho_g \triangle V}{\triangle t} + \mathbf{a_E} + \mathbf{a_W} + (\varepsilon\rho_g \mathbf{U} A)_e - (\varepsilon\rho_g \mathbf{U} A)_w + \rho_g A_{surf} h_m$
$\mathbf{S_u}$ (cell center)	$\frac{\varepsilon\rho_g^o Y_{j,p}^o \triangle V}{\triangle t} + S_{y,j} \triangle V$
$\mathbf{S_u}$ (internal cells)	$\frac{\varepsilon\rho_g^o Y_{j,p}^o \triangle V}{\triangle t} + S_{y,j} \triangle V$
$\mathbf{S_u}$ (cell surface)	$\frac{\varepsilon\rho_g^o Y_{j,p}^o \triangle V}{\triangle t} + S_{y,j} \triangle V + \rho_g A_{surf} h_m Y_{j,\infty}$

TABLE 3.7: A solution to the discretized pressure-correction equation.

Coefficient	Solution of the pressure-correction equation.
$\mathbf{a_W}$	$\frac{\eta}{\mu\triangle r}(\rho_g A)_w$
$\mathbf{a_E}$	$\frac{\eta}{\mu\triangle r}(\rho_g A)_e$
$\mathbf{a_P}$	$\mathbf{a_E} + \mathbf{a_W}$
$\mathbf{S_u}$	$\frac{\rho_g \triangle V}{\varepsilon} - \frac{(\rho_g - \rho_g^0)\triangle V}{\triangle t} + (\rho_g A \mathbf{U}^*)_w - (\rho_g A \mathbf{U}^*)_e$

Here it must be noted that the correction pressure P′ is defined as a difference between correct pressure field, P and the guessed pressure field, (P*). The same is true for the velocity field, as shown below,

$$\begin{aligned} P &= P^* + P' \\ \mathbf{U} &= \mathbf{U}^* + \frac{\eta}{\mu\triangle r}(\mathrm{P}'_{\mathrm{i}} - \mathrm{P}'_{\mathrm{i+1}}) \end{aligned} \tag{3.18}$$

The indexes i and $i+1$ denote the current control volume and its east neighbor control volume, respectively.

3.4 Iterative procedure

Once the appropriate equations, the boundary and initial conditions are set; the solution methods involve an iterative scheme to arrive at simulation results. Since the system of PDE's is nonlinear, several iterations must be carried out during each time step of the numerical solution until convergence is reached.

During the iterative convergence, some criteria may need to be fulfilled and it is usually defined by acceptable error in some parameter values. It is also important to examine whether the final time has been reached with proper convergence at each time step. Figure 3.3 shows the iterative procedure used to obtain numerical solution for the particle model.

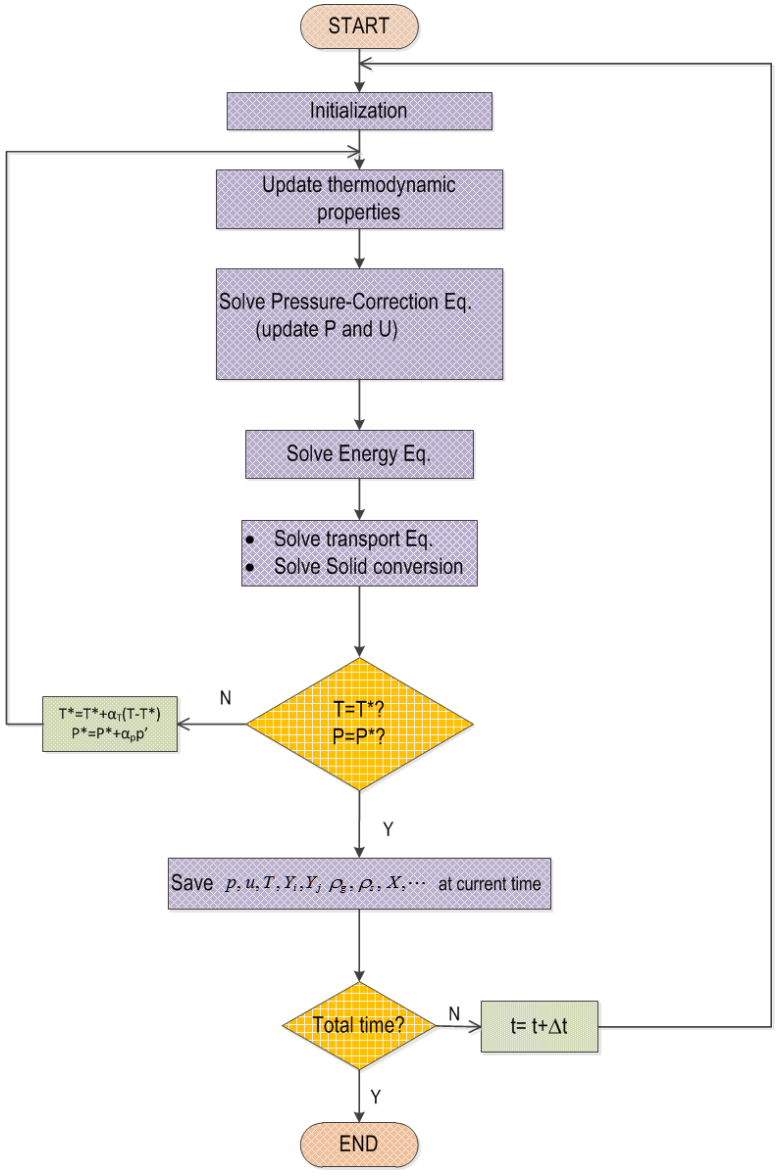

FIGURE 3.3: Overall algorithm for the sequence of operations in the problem

3.5 Modeling tools: C++ and gPROMS ModelBuilder

For simulating the calcination process of kaolinite clay particle, a stand alone C++ code has been successfully developed; the same process has also been simulated in a commercial software called gPROMS.

- The model developed in c++ for single clay particle calcination is not only to achieve a better understanding of the conversion process of a single clay particle when it is suddenly exposed to a known calcination condition, but also to be integrated, after proper reformulation, into advanced CFD simulations of the reacting particulate flow system in the calciner later. CFD simulation of the entire calciner is crucial in order to really understand its performance and ultimately to come up with innovative conceptual design of smart and energy-efficient calciners.
- The ultimate purpose of using gPROMS here is for the calcination plant performance evaluation and optimization by modeling the calciner and integrating the calciner model into the whole system in the plant. Even though such a plan was changed by the project consortium during the project, the comparison between the standalone c++ code and commercial gPROMS can serve as a kind of model cross-validation.

gPROMS is a commercial software abbreviated for general PROcess Modeling System. It is a bundle of software tools with a common solver kernel to compute numerical solutions and optimization problems [Pantelides and Barton, 1993]. These are created in a central graphical user interface (GUI) which is called ModelBuilder. This tool can also be used to start certain tasks, analyze and view results. Modeling and Simulating in gPROMS are done by setting up different objects called entities with dedicated purposes [Oh and Pantelides, 1996; Pantelides and Barton, 1993; PSE, 2013]. For instance, gPROMS ModelBuilder requires to have at least the VARIABLE TYPE, MODEL and PROCESS entities. The upper and lower bounds of a variable are declared under the entity VARIABLE TYPE. The set of equations, assignments, parameters and initial conditions together with event conditions are specified under the entity MODEL. Several models can also be written and coupled to each other without worrying about their hierarchy. The PROCESS entity is the main task that controls simulation activities, furthermore, this entity includes assignment of parameters, specification of initial conditions and setting solver parameters. Figure 3.4 illustrates a screenshot of a well posed calcination model and gPROMS ModelBuilder interface along with visualization of output results.

gPROMS uses a number of state-of-the-art hierarchical solvers. Among these are, DASOLV for Differential-Algebraic Equations, BDNLSOL for Nonlinear Equations and the MA28 and MA48 for sparse linear system of equations.

Although this study is not intended to compare the two modeling tools, the major differences in using C^{++} code and gPROMS to simulate the calcination process are highlighted as follows;

- While C++ needs to discretize the geometry and the governing equations manually, gPROMS handles it by simply specifying the method of discretization and its order of accuracy.
- C++ needs to write the final discretized equations in a standard form [Patankar, 1980; Versteeg and Malalasekera, 2007] so that it would be convenient to solve by Tri-diagonal matrix algorithm (TDMA) or Thomas algorithm; whereas gPROMS needs to write the equations as they appear in paper [PSE, 2013] and the mathematics is handled by built-in solvers.
- While convergence and computational stability needs much effort in C++; initialization and setting well posed system is the most difficult task in gPROMS.

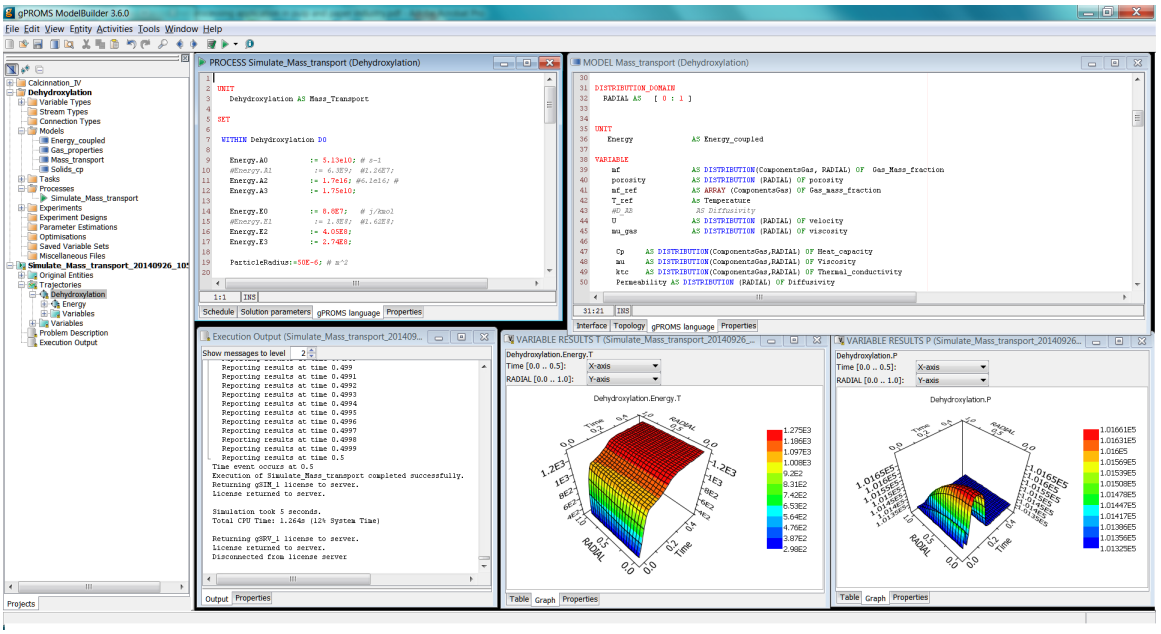

FIGURE 3.4: A screenshot of gPROMS interface

Chapter 4

Experimental study

The experiments under this section not only provide a detailed data on the initial composition and property of the kaolinite rich clay material, but also offer an in-depth understanding on the thermal calcination of kaolinite rich clay sample into different products under different calcination conditions. This chapter, therefore, is dedicated to the experimental study performed to determine kinetic parameters, characterize the composition, specific density, PSD and other physical properties of the clay material under investigation. The outcome from the experiments is used as an input for modeling study or model validation.

4.1 Study of kinetic parameters

The kinetic parameters (A and E) of dehydroxylation of kaolinite rich clay particles are determined by using the well known Kissinger's approach [Kissinger, 1957, 1956], using thermogravimetric experiments. The method is based on the shift in peak temperature (the temperature at which the reaction rate is maximum), when a reaction occurs at different heating rates. The shift in peak temperature is clearly shown in in Figure 4.1 when DTA experiments are performed at different heating rates for kaolinite rich clay sample.

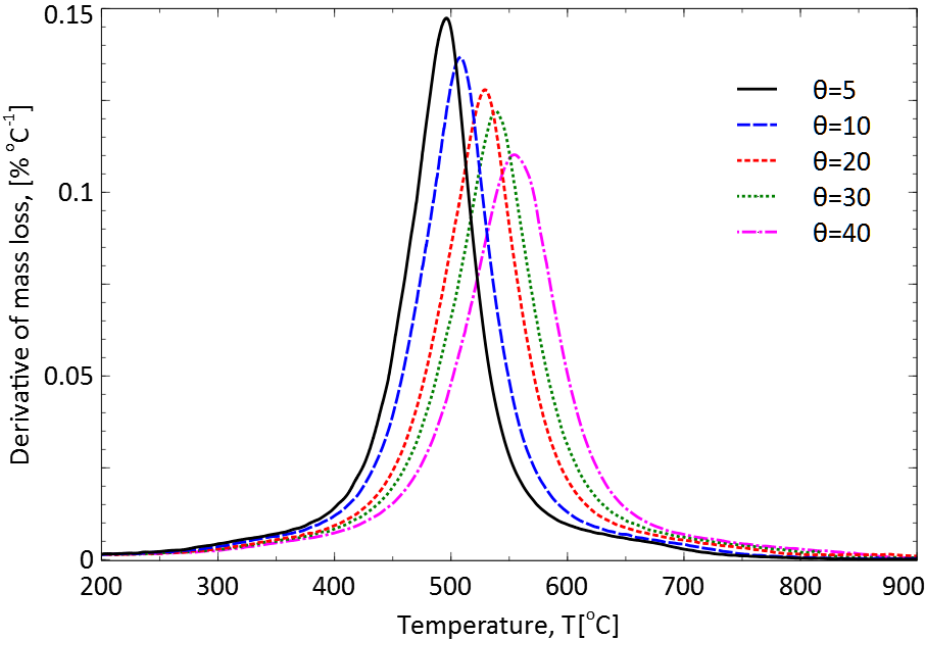

FIGURE 4.1: The shift in temperature during dehydroxylation of kaolinite rich clay at different heating rates, θ (°C/min)

In order to summarize the derivation of Kissinger's equation briefly, we begin with the general expression of decomposition reaction as,

$$\frac{d\alpha}{dt} = kf(\alpha) \tag{4.1}$$

where α is the the degree of dehydroxylation, k is the rate constant, and $f(\alpha)$ is a kinetic model that dictates the behavior of the dehydroxylation reaction.

According to Kissinger, the the kinetic model is represented by order based kinetics, where $f(\alpha) = (1-\alpha)^n$. Hence, the above equation is rearranged into:

$$\frac{d\alpha}{dt} = k(1-\alpha)^n \tag{4.2}$$

where n is the empirical kinetic exponent of the reaction. Substituting the rate constant, k with Arrhenius relationship and rearranging and integrating the equation gives the final Kissinger's expression as shown in Eq. 4.3. Further information on the derivation of the method can be referred in the literature [Chen et al., 1993; Kissinger, 1957, 1956; Llópiz et al., 1995; Ptáček et al., 2011].

$$ln\left(\frac{\theta}{T_p^2}\right) = -\frac{E}{RT_p} + ln\left(\frac{AR}{E}\right) \tag{4.3}$$

where, θ is the heating rate (K/min) and T_p is the maximum reaction rate temperature (K). The plot $ln(\theta/T_p^2)$ versus $1/T_p$ is a straight line whose slope is $-E/R$ and an

intercept $ln(AR/E)$. Although the method has been criticized and modified by several authors [Baumann et al., 2010; Boswell, 1980; Sesták et al., 2014], it still remains popular to determine kinetic parameters of decomposition reactions and other solid-gas reactions.

The kinetic exponent or Avrami's constant (n) has also been calculated based on the characteristics of the DTG curve [Augis and Bennett, 1978], where its value is approximated as:

$$n = \frac{2.5RT_p^2}{W_{1/2}E} \tag{4.4}$$

The reaction mechanism has been interpreted based on the value of Avrami's constant, as it is commonly practiced in literature [Criado et al., 1984; Hankock and Sharp, 1972; Ptáček et al., 2011; Saikia et al., 2002].

4.1.1 Thermogravimetric study

Dehydroxylation of kaolinite clay is carried out by using thermogravimetry method. It simultaneously measures both the heat flow (DSC) and weight changes (TGA) associated with transitions in a material as a function of temperature and time in a controlled atmosphere. The general procedure of the test is described as follows. Approximately about 20 mg (± 2) of clay sample is placed in a Pt crucible. The sample is heated to a maximum temperature of 1373 K at different heating rates (5, 10, 20, 30, 40 and 50 K/min) in nitrogen environment at flow rate of 100 cm^3/min. Relevant data are collected, in which the weight loss from TGA and its derivative DTG are plotted against temperature, as shown in Figure 4.2. Moreover, the DTG data were analyzed to extract the peak temperature (T_p) and the half peak width ($W_{1/2}$).

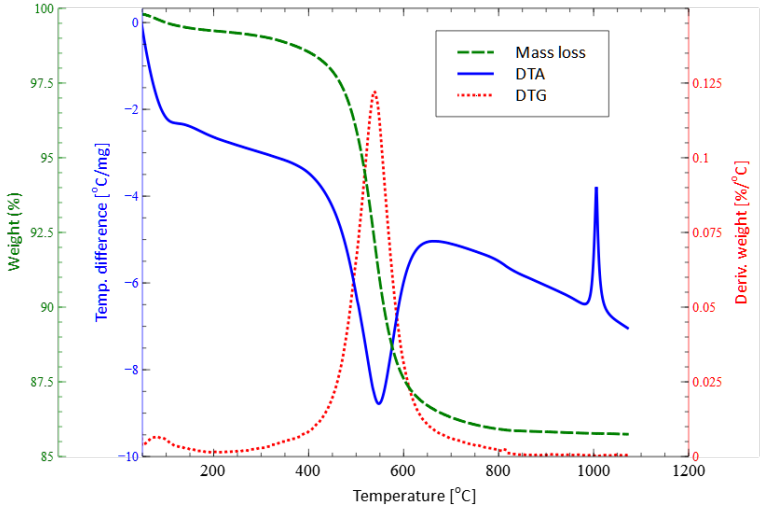

FIGURE 4.2: A representative thermogram for an experiment done at a heating rate of 20 K/min

Two TGA experiments are carried out utilizing different TGA models. The first experiment is done using model SDT 2960 and the second is STA 409 PC, which are illustrated in Figure 4.3. The same procedure is used for both experiments except that the sample size is well controlled for each test in the second experiment.

FIGURE 4.3: TGA equipment used during study

The DTG curve for each test is examined to derive useful information such as the peak temperature, the half width maxima ($W_{1/2}$) and the values of kinetic exponent (n). The Experimental peak characteristic values obtained from DTG curve at different heating rates are shown in Table 4.1 and 4.2.

TABLE 4.1: Experimental peak characteristic values from Experiment 1.

θ (K/min)	T_p (K)	$W_{1/2}$	n
5	769.6	64	1.1
10	785	69	1.04
20	805	75.1	1.03
30	815.32	78.5	1.02
40	828.6	85.2	1.0

TABLE 4.2: Experimental peak characteristic values from Experiment 2.

θ (K/min)	T_p (K)	$W_{1/2}$	n
5	778	66	1.28
10	795.5	70.1	1.24
20	816.4	72.3	1.22
30	825	74.2	1.21
40	832.15	80.5	1.12
50	837.6	81.7	1.12

Based on experimental results collected for TGA experiments, the plot $ln(\theta/T_p^2)$ versus $1/T_p$ is illustrated in Figure 4.4, where the activation energy is calculated from the slope.

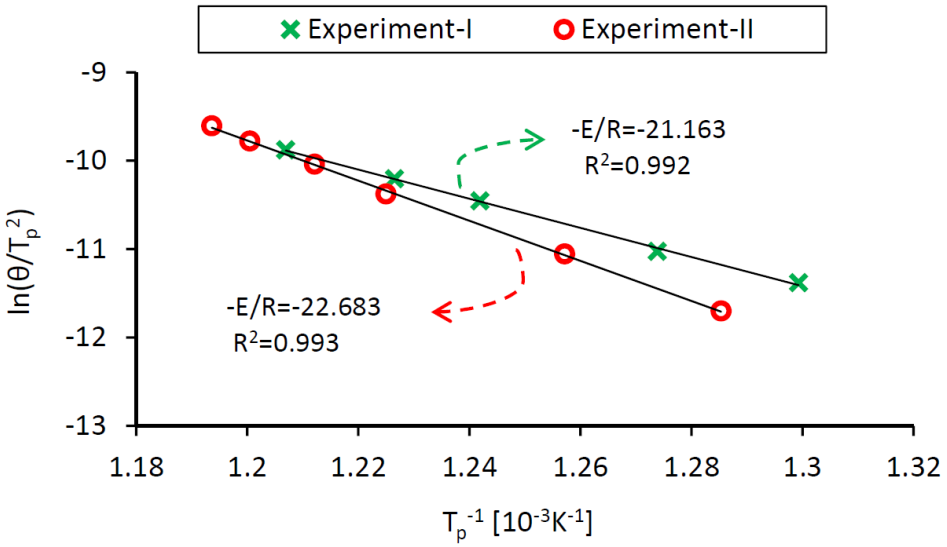

FIGURE 4.4: Plot of $ln(\theta/T_p^2)$ versus $1/T_p$ to determine kinetic parameters

4.2 Gas Suspension Calciner (GSC)

The calcination test is performed in a gas suspension calciner located in FLSmidth R& D Center Dania (Denmark). The schematic sketch of the GSC is illustrated in Figure 4.5. The main objective of this test is to examine the property of calcines after it gets exposed to various calcination temperatures. For this purpose, a dried and crushed kaolinite rich clay sample is used as a feed material with initial composition of 90-95 % kaolinite and 5-10 % quartz. The feed has particle size distribution as shown in Figure 4.6.

The feed material is introduced into the system at a feeding rate of 6 kg/hr. The hot gas generated in the main burner is drawn into the calciner from the bottom and pulled through the reactor tube together with the feed particles by an extraction fan. The hot gas/particle flow is mixed with a stream of quenching air at the exit of the GSC, and finally enters the filter to separate the product from the gas flow.

The system has provision of secondary burners that may be put into operation to obtain a uniform temperature profile in the calciner. Hence, two sets of experiments are performed. The first sets of experiments are accomplished without support burners where calcination tests under 1073, 1173, 1273 and 1373 K are performed. During this test a temperature drop was noticed along the calciner. The temperature across the calciner is measured with the help of thermocouples that are put at four different locations along the GSC. The second set of experiments are performed by using support secondary burners to maintain constant calcination temperature at 1073 and 1273 K all over the calciner.

In all of the six tests made, the clay particles are expected to have about 0.5 s residence

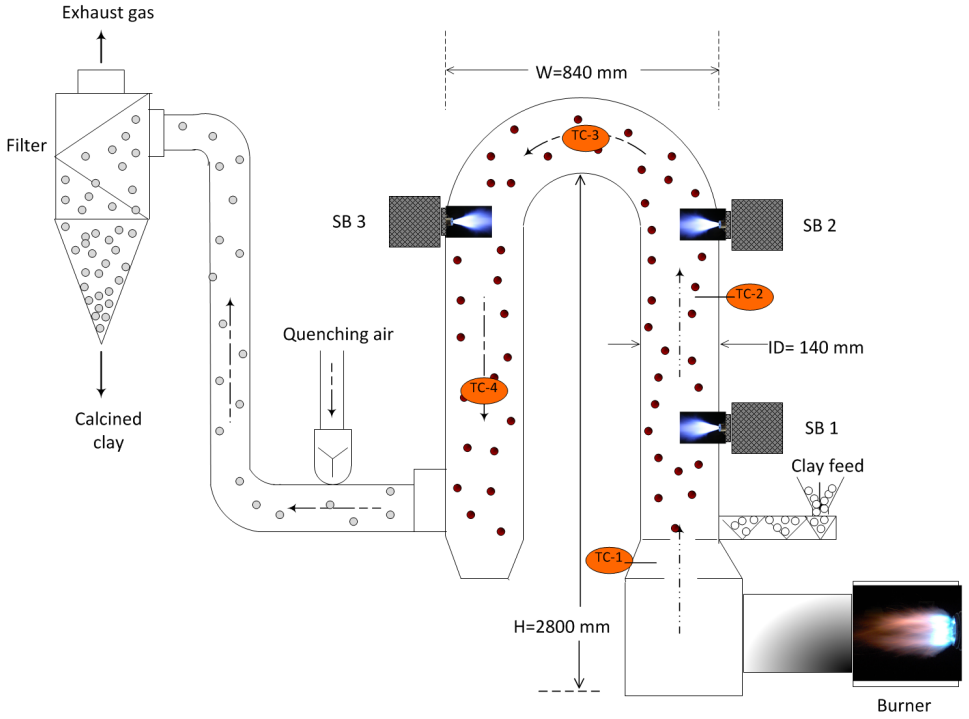

FIGURE 4.5: A schematic sketch of the gas suspension calciner along with the position of secondary burners (SB) and thermocouples (TC).

time inside the calciner. The calcined clay material is then collected after each test for further analysis. Table 4.3 presents the calcination conditions for the experiments carried out in GSC and detailed description of each experimental setup and sample ID. Those experiments carried out when secondary burners are not operational (EXP-I) exhibit a significant temperature drop along the calciner. When secondary burners are operational (EXP-II), the temperature inside the GSC is observed to be stable.

TABLE 4.3: Calcination conditions of the GSC and details of sample ID

Test	Calcination temperature (K)		Secondary	Calcined	Temperature drop (K)			
	Nominal	Average	burners	product ID	TC-1	TC-2	TC-3	TC-4
Exp-I	1073	964	NO	$MK964_{NB}$	1067	979	921	893
	1173	1058	NO	$MK1058_{NB}$	1168	1078	1022	972
	1273	1126	NO	$MK1126_{NB}$	1269	1158	1062	1012
	1373	1214	NO	$MK1214_{NB}$	1362	1244	1147	1081
Exp-II	1073	1073	Yes	$MK1073_{WB}$	1075	1070	1062	1061
	1273	1273	Yes	$MK1273_{WB}$	1271	1276	1263	1264

4.3 Characterization test of the raw feed and the calcines

Today, the significant advance in X-ray diffraction (XRD) and X-ray fluorescence (XRF) techniques enabled to fully characterize clay minerals [Bish and Post, 1993; Chung and

Smith, 1999; Snellings et al., 2010]. However, the complex nature of clays make characterization difficult and thus, it needs to be supplemented with other methods for accurate quantification. This section presents different characterization tests that have been made to fully characterize both the feed and the calcined clay material.

4.3.1 Mineralogical composition and PSD

The mineralogy of the clay material under investigation is determined by a combination of results from chemical analyses by X-ray fluorescence and X-ray diffraction on both oriented and random powder samples, supplemented with other thermal methods such as thermogravimetry.
The kaolinite rich clay sample has chemical composition as shown in Table 4.4. This clay sample is pretreated and conditioned prior to using it as feed material. The treatments are usually physical and doesn't affect the composition of the clay sample.

TABLE 4.4: Chemical composition of kaolinite rich clay sample

Chemical composition, wt.%								
SiO_2	Al_2O_3	Fe_2O_3	CaO	TiO_2	P_2O_5	K_2O	Na_2O	LOI
47.9	35.06	0.77	0.2	1.29	0.11	0.12	0.06	13.65

The particle size distribution of the clay sample is measured using Malvern equipment with laser diffraction by measuring the angular variation in intensity of light scattered when a laser beam passes through a dispersed clay sample. It is based on the principle that particles passing through a laser beam will scatter light at an angle that is directly related to their size: large particles scatter at low angles, whereas small particles scatter at high angles. Thus, a collection of particles will produce a pattern of scattered light defined by intensity and angle that can be transformed into a particle size distribution. The PSD of the feed and calcined clay is illustrated in Figure 4.6.

4.3.2 Density and surface area

The density of the feed clay material and the calcined clay material has been measured by Gas Pycnometer Micromeritics, AccuPyc II 1340. The measurement and principles are based on gas displacement method to measure volume accurately. An inert gas, helium, is used as the displacement medium. The clay sample is sealed in the instrument compartment of known volume, the appropriate inert gas is admitted, and then expanded into another internal chamber. The pressure difference before and after expansion helps

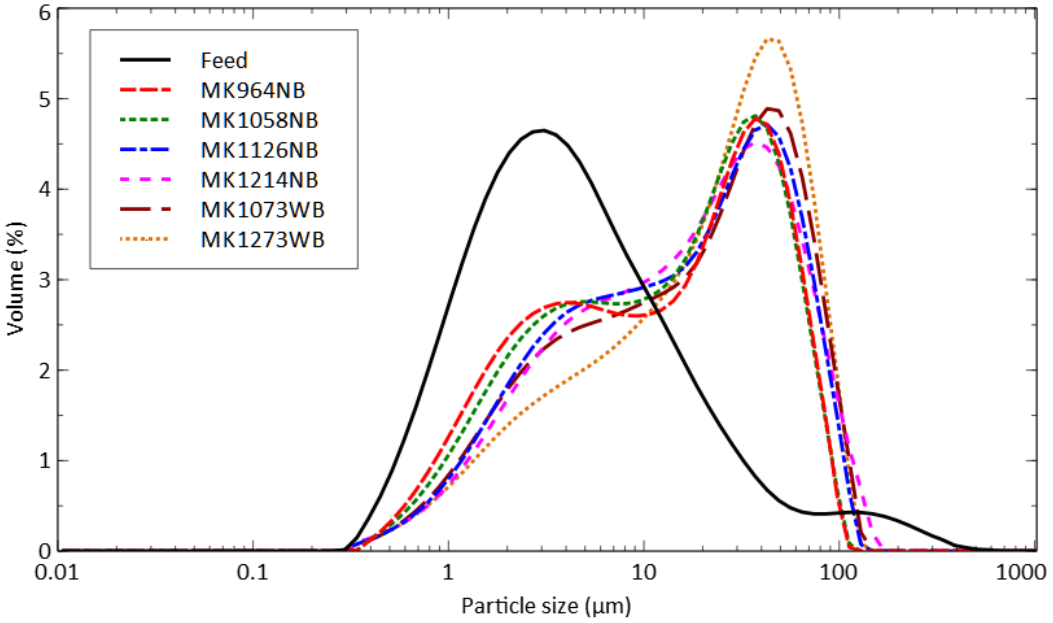

FIGURE 4.6: Particle size distribution of the feed and calcined clay materials.

to compute the sample volume. The density is then calculated by dividing the sample weight by its volume.

Surface area of the feed and calcined clay material is measured using BET method which is based on the adsorption of gas on a surface. The amount of gas adsorbed at a given pressure allows to determine the total specific surface area in m^2/g.

4.3.3 Degree of dehydroxylation

The degree of dehydroxylation of the clay sample is studied by using LECO RC612 multiphase carbon and hydrogen/moisture analyzer shown in Figure 4.7. The equipment features a state-of-the-art furnace control system, allowing the temperature of the furnace to be programmed from near-ambient to 1373 K. The main purpose of this experiment is to examine the degree of conversion or dehydroxylation by monitoring the amount of crystal water in the clay sample.

The principle is based on examining the mass of water left after the clay sample has been heated to high temperature inside the equipment. For such purposes, 250 mg of the feed clay is placed into a system stabilized with inert nitrogen atmosphere. The raw feed clay sample is held at 423 K for 15 minutes to make sure that the free water is removed. Then, the clay sample is exposed to a heating rate of 120 K/min until 1273 K and held at this temperature for about 7 minutes to secure a complete dehydroxylation (i.e., a complete removal of the crystal water). A built-in Infrared detection method is

used to quantify the amount of vapor as a weight percentage. The same procedure is repeated for calcined samples. The final output from the instrument gives the amount of water vapor in weight percentage, as shown in Figure 4.8.

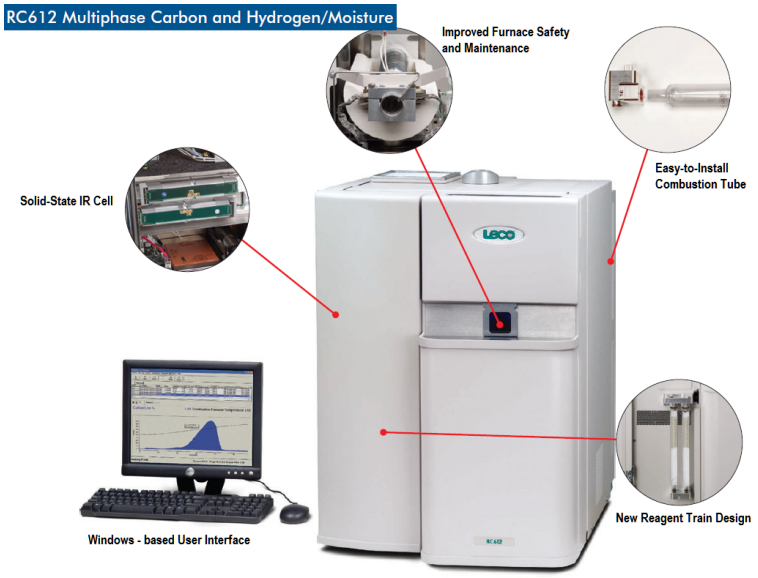

FIGURE 4.7: LECO RC612 Multiphase Carbon and Hydrogen/moisture analyzer.

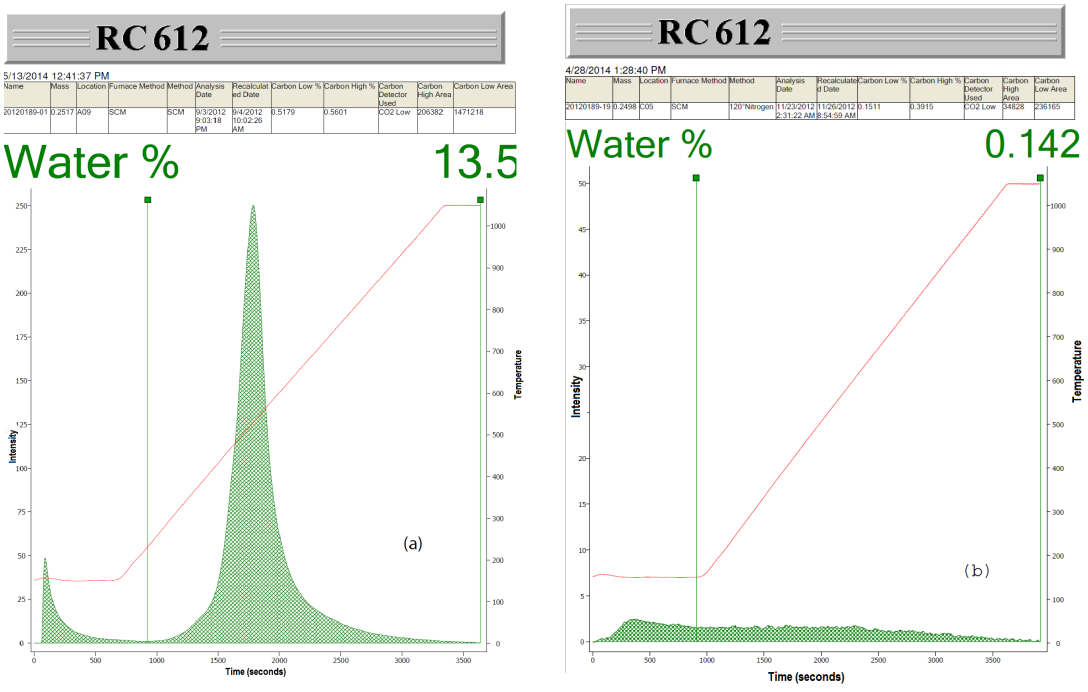

FIGURE 4.8: The amount of vapor in terms of weight fraction, as it is shown in LECO RC612: (a) Feed (b) calcined clay at 1273 K ($MK1273_{WB}$)

Finally, the degree of dehydroxylation, α is determined by comparing the crystal water left in each calcined sample (m_{CS}) to the initial amount of crystal water in the raw feed (m_{RF}), as shown in Eq. 4.5. When all crystal water is removed from the calcined sample, the amount of water left (m_{CS}) approaches to zero and hence degree of dehydroxylation,

α becomes closer to 1.

$$\alpha = 1 - \frac{m_{CS}}{m_{RF}} \tag{4.5}$$

A summary of the vapor signals for all clay samples is illustrated in Figure 4.9, where the intensity of water vapor evolved from the feed and calcined clays are plotted against temperature. The observed decreasing trend in the intensity of vapor is due to the fact that the calcination process in the GSC has driven out most of the crystal water from the clay material.

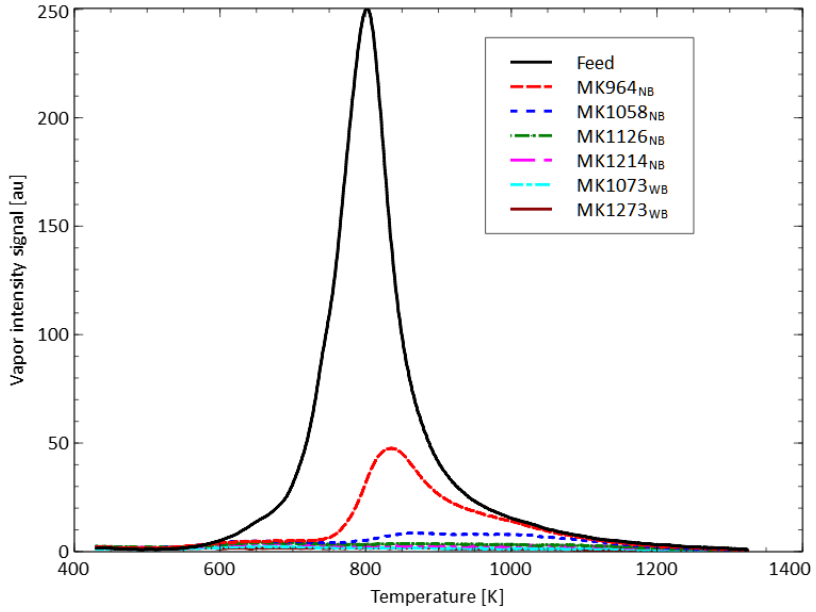

FIGURE 4.9: A graphical plot of the intensity of vapor during LECO RC612 thermal analysis for the feed and calcined clay products.

4.3.4 Composition of phases

X-ray diffraction is by far the commonest method used to determine the amount of phases in clay sample. In this study, XRD is used to determine the qualitative and quantitative phase analysis of clays. The analysis of the as-received and calcined samples is carried out using PANalytical CubiX PRO X-ray diffractometer as illustrated in Figure 4.10. Rietveld analysis of randomly oriented clay powders is used to quantify the composition of the calcined clay material after each run at its respective calcination temperature. Quantification of phases is based on the comparison of the mass fraction of each component with a known standard [Bish and Post, 1993], where 10 % anatase (TiO_2) is used as internal standard.

FIGURE 4.10: The PANalytical CubiX PRO X-ray diffractometer used in this study.

Since X-ray diffraction determine the relative amount of each phase by comparing the positions and intensities of the diffraction peaks against a library of known crystalline materials, having known the amount of crystalline phases in the calcined material, the amorphous material (metakaolinite) can be approximated indirectly as:

$$Y_{am} = 1 - \sum_{i} Y_{i,c} \tag{4.6}$$

where Y_{am} is mass fraction of amorphous material and $Y_{i,c}$ is the mass fraction of crystalline phases in the calcined clay material. The approximated mass fraction of the amorphous material may not entirely be metakaolinite, some unidentified none crystalline materials may share some part; for instance amorphous silica. It is known that the clay material under study is rich in kaolinite with some quartz impurities. Since kaolinite, quartz and mullite phases are crystalline they can be easily quantified with XRD as shown in Figure 4.11. Based on this quantification, the amount of amorphous phase (metakaolinite) is reasonably approximated.

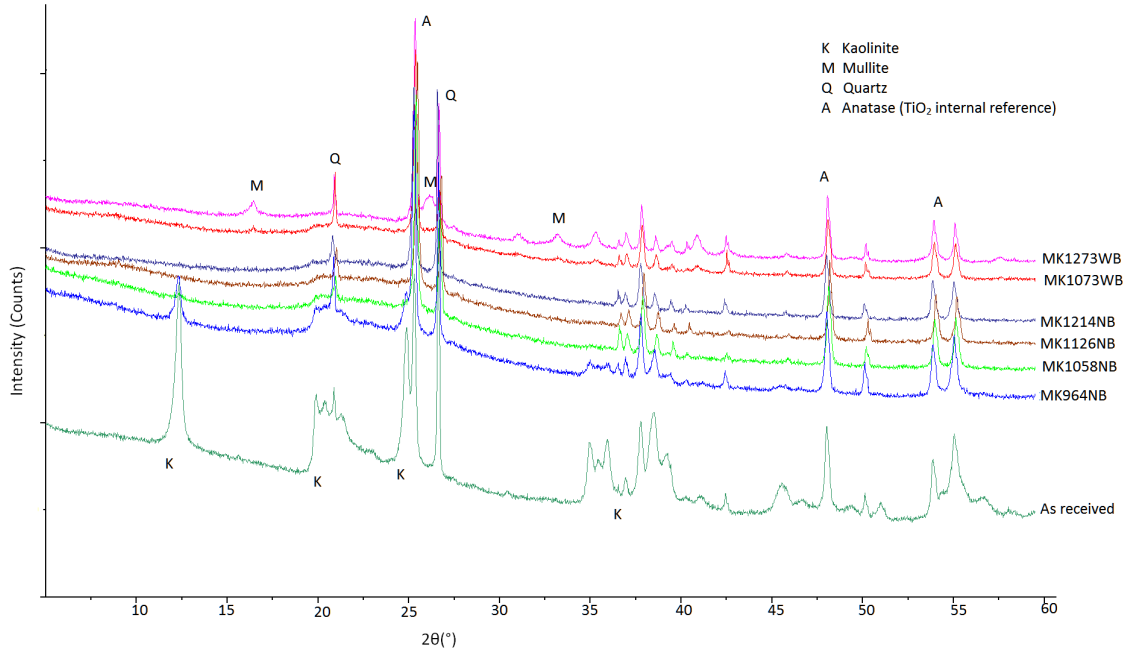

FIGURE 4.11: XRD pattern of the as received clay sample and its calcines at different calcination temperature.

Chapter 5

Result and discussion

This chapter presents the outcome of the study supplemented with discussions in relation to the available literature. Results are presented in different sections where the values of kinetic parameters are computed, comparison of experimental data with model prediction are established and composition of phases are explained. Lastly, a detailed results predicted by the model at different calcination conditions are presented, with brief sensitivity analysis on the impact of the most important calcination conditions such as gas temperature, residence time and kinetic parameters.

5.1 Kinetic parameters

Based on the experiments performed in chapter 4, kinetic parameters for kaolinite dehydroxylation reaction are determined. The calculated experimental values of kinetic parameters are given in Table 5.1 along with the "average" value which is explained in *Paper 2*. Other kinetic parameters collected from literature are also given in the same table for comparison purposes. Generally, the values are so diverse that they can influence the rate of reaction significantly. Figure 5.1 illustrates the impact of kinetic parameters on the rate constant, k, which is expressed in terms of Arrhenius relationship as, $k = A_i exp(-E_i/RT)$.

TABLE 5.1: A summary of kinetic parameters for kaolinite dehydroxylation from literature and experimental values of this study

E(kJ/mol)	A($s^{-}1$)	Method	Source	Reference
177	4.57×10^{8}	Thermal Analysis, DTA	Florida, USA	[Kissinger, 1956]
193	1.0×10^{9}	Thermal Analysis, TGA	Georgia, USA	[Bellotto et al., 1995]
196	9.6×10^{8}	Thermal Analysis, TGA	India	[Saikia et al., 2002]
195	8.58×10^{14}	Thermal Analysis, DTG	Rep. Czech	[Ptáček et al., 2011]
163	2.0×10^{12}	Thermal Analysis, TGA	USA	[Levy and Hurst, 1993]
176	1.66×10^{11}	TGA, SDT 2960	EU	Experiment-I
189	2.7×10^{9}	TGA, STA 409 PC	EU	Experiment-II
180	6.3×10^{9}	–	EU	Average value

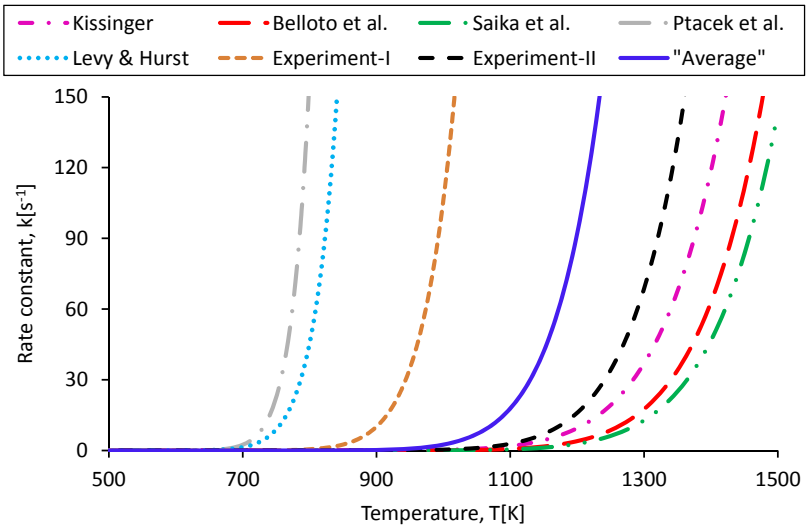

FIGURE 5.1: The influence of kinetic parameters on the rate constant

Although the experiment is aimed at estimating the kinetic parameters quickly, different values of activation energy and frequency factor are obtained for each experiment, but within the range of values given in literature. A possible reason for the variation could be the interdependency among the different factors considered. The sample mass, sample particle size and packing [Schilling, 1990] are among the factors that may affect the shape, precision and accuracy of the experimental results in thermogravimetry. The sample mass might cause sample temperature to deviate from a linear temperature change affecting the shape of thermogram during experiment. The particle size may also cause a change in the diffusion of the evolved gases during reaction which alters the reaction rate and hence the shape of the DTG curve [Stoch, 1984; Stoch and Waclawska, 1981]. Apart from the above mentioned reasons, the different values of kinetic parameters obtained above could also be due to the uncertainty associated with the method itself, which has been under debate in literature [Michèle et al., 2011; Opfermann and Flammersheim, 2003; Pijolat et al., 2005; Sesták et al., 2014].

5.2 Experimental and modeling results of flash calcination in the GSC: A comparison

As a first effort to validate the model, TGA experiments are used to compare the conversion profile with model results. The details can be seen in *Paper 1*, where further explanation on the little discrepancy observed at higher degree of conversion are made.

The other major effort to validate the model results is using experimental results from the pilot scale GSC. *Paper 2* describes in detail the comparison between the GSC experimental data and model predictions.

The process conditions inside the GSC are taken into account in the model. There are two parameters that need attention: the particle size and calcination temperature. The implementation of the real particle size and real temperature during calcination is essential to fairly generate representative results. The particle size is implemented based on the PSD of the feed material (see Figure 4.6), from which 6 representative particle sizes are finally used (with proper volume percentages) in the model. The calcination temperature is implemented based on the temperatures measured at different position in the GSC. Thus, a piecewise-linear temperature profile is implemented in the model. Detailed description of such implementation can be found in *Paper 2*.

For those tests done in the presence of secondary burners (Exp-II), the temperature profile along the GSC is nearly constant and uniform. As a result, the nominal calcination temperature is implemented directly in the model.

Under the above calcination conditions and proper implementation of temperature and PSD, model results are compared with experimental data. The density and degree of dehydroxylation are good indicators to evaluate structural changes during the course of calcination [Davies, 1986; Slade and Davies, 1991]. Hence, a comparison in density is illustrated in Figure 5.2.

As shown in Figure 5.2, when kaolinite rich clay particles are flash calcined at a given calcination temperature for about 0.5 seconds, it displays a drop in density of the calcined material at lower calcination temperatures ($MK964_{NB}$ and $MK1058_{NB}$) and then density increases with calcination temperature. Such observation is common among flash calcined kaolinites [Bridson et al., 1985; Slade and Davies, 1991], even soak calcined kaolinites display similar trend in density [Grim, 1953]. When kaolinite is exposed to temperatures 900 – 1200 K, it tends to lose the structural hydroxyls to form a poorly ordered structure, metakaolinite. This material is characterized by amorphicity and low density [Davies, 1986]. As calcination temperature increases, a slow increase in density is observed which is due to the rearrangement of alumina and silica structures to form a

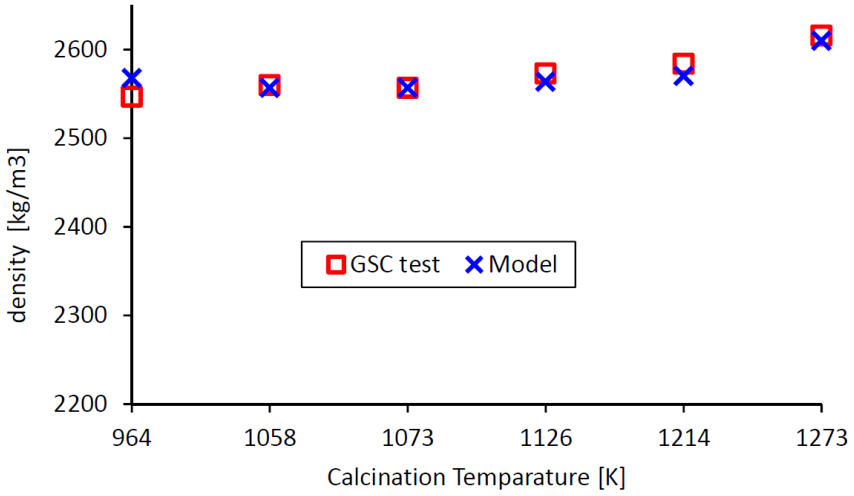

FIGURE 5.2: Comparison between GSC tests and model predictions: density of the clay samples

dense mullite phase. The X-ray pattern observed for the calcined products in Figure 4.11 is a good indication for the formation of mullite phase at higher calcination temperature ($MK1273_{WB}$).

The degree of dehydroxylation, α which implies the amount of crystal water removed after the kaoilinite rich clay material has been exposed to various calcination conditions, is also another parameter that is used to compare experimental data with model prediction. The degree of dehydroxylation of the calcined clay at different calcination temperatures is compared with model results. Figure 5.3 presents a comparison between the experiments and model prediction.

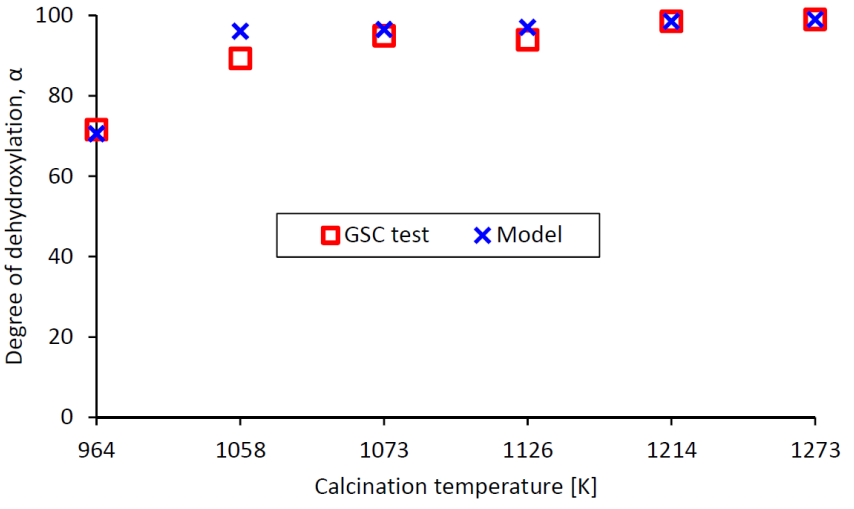

FIGURE 5.3: Comparison between GSC tests and model predictions: Degree of dehydroxylation

Despite the presence of some uncertainties associated with the operation of GSC such as temperature drop along the GSC, the above comparison is generally found to be in good agreement.

Other experimental data that need to be discussed is, the composition of phases after the feed clay material has been exposed to different calcination conditions. As it is described in the previous chapter, XRD and XRF have been a prominent tools to estimate the mineralogical composition and the amount of phases in the clay sample. The estimation is made by Rietveld refinement of randomly oriented samples using the known mineralogy of the feed clay material as input. As shown in Figure 4.11, it is clear that the diffraction signals from kaolinite decreases as the the calcination temperature increase. This is due to transformation of kaolinite into other phases, mainly to metakaolinite. Unfortunately metakaolinite is amorphous phase and is not shown in the XRD pattern but can be estimated indirectly. Another interesting observation from the XRD pattern is, the formation of mullite is not shown for all calcined products, except for those samples exposed to temperatures about 1273 K in the presence of secondary burners ($MK1273_{WB}$). This implies that all other calcination temperatures are safe but may not cause complete transformation of kaolinite to metakaolinite at the given residence time.

Table 5.2 compares the composition of phases in the calcined clay materials with model prediction. A detailed analysis on the comparison of phase composition between the experiments and model can be found in *Paper 2*. Such comparison must account the uncertainties associated with XRD method, such as, use of anatase as a reference, weighing of samples, peak-overlap, low signal/noise ratios and poor simulations in Rietveld XRD.

TABLE 5.2: Experimentally estimated and model-predicted composition of clay samples

Sample	Kaolinite (%)		Quartz (%)		Amorphous (%)		Mullite (%)	
	Experiment	Model	Experiment	Model	Experiment	Model	Experiment	Model
Feed	90-95	94	5-10	6	-	-	0	0
$MK964_{NB}$	10*	31.1	6	6.6	84*	63	0	0
$MK1058_{NB}$	1	2.5	8	7	91	90.4	0	0
$MK1126_{NB}$	0	1.23	9	7.7	91	90	0	0
$MK1214_{NB}$	0	0	9	8.9	91	87	0	1.05
$MK1073_{WB}$	0	1.2	8	7	92	90.1	0	4.02
$MK1273_{WB}$	0	0	10	13.7	74	71.76	16	14.4

∗Thermal analysis suggests 27% of kaolinite for MK964NB which leaves the amorphous content to be 66%

A cross-comparison between the C++ model and gPROMS results is also made, as a kind of model validation effort. The agreement between the two modeling tools verifies the mathematical approach of the model. Figure 5.4 illustrates the comparison of model output in C++ and gPROMS, where the temperature profile and the conversion are compared. Detailed results based on gPROMS ModelBuilder can be found in *Paper 3*.

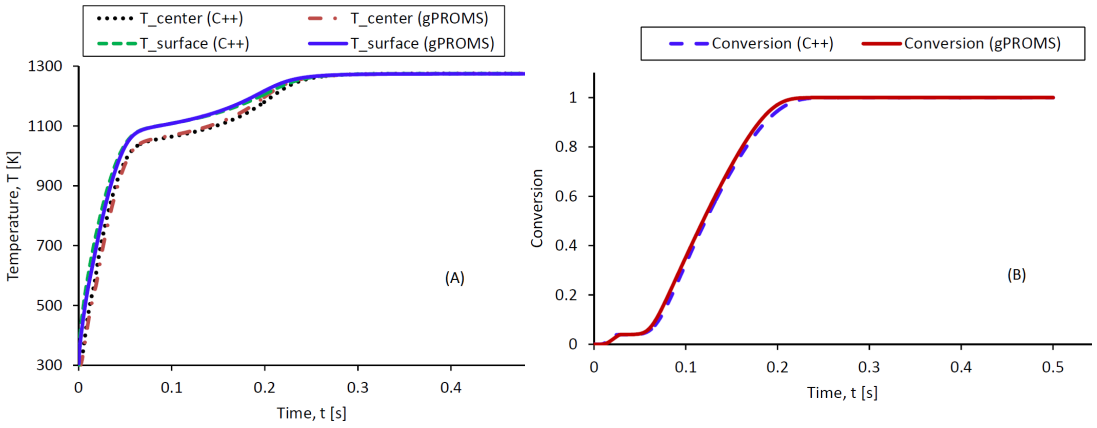

FIGURE 5.4: The comparison between C++ and gPROMS results (A) temperature profile at particle center/surface (B) model predicted conversion profile

5.3 Detailed model prediction

5.3.1 Baseline case results

The following detailed explanation on model results is based on the calcination conditions given in Table 5.3. Since most physical properties are adopted from the bulk properties of kaolinite clay powder, a spherical kaolinite clay particle having a diameter of 100 µm is assumed. The model results explained here are similar to those explained in *Paper 1* and *Paper 2*, except that larger particle size and "average" kinetic parameters are used to simulate the current results.

TABLE 5.3: The initial properties of kaolinite clay and calcination conditions

Variables	Values
Initial density of feed clay particle	2654 kg/m^3
mass fraction of kaolinite in particle	93%
mass fraction of silica in particle	6.1%
mass fraction of moisture in particle	0.9%
Initial temperature of clay particle, T_0	298 K
Clay particle diameter, D_p	100 µm
Biot number, B_i	$h_T D_p/6k$
Pore diameter, d_p	3×10^{-7} m
Porosity, ε	0.5
Ambient gas composition	Air (77 wt.% N_2 and 23wt.% O_2)
Ambient gas temperature, T_∞	1273 K
Radiation temperature, T_{rad}	$T_{rad} = T_\infty$
Ambient gas pressure, P_{atm}	101,325 Pa

When a kaolinite particle is plunged into a hot air at temperature 1273 K, it undergoes a sequence of transformations where the heat and mass transfer profile is given in Figure 5.5. As shown in the figure, the particle surface temperature is remarkably higher than the temperature in the center. This is due to convective and radiative transfer of heat from the surrounding to the particle surface which then transfers to the center by conduction until the particle attains isothermal condition.

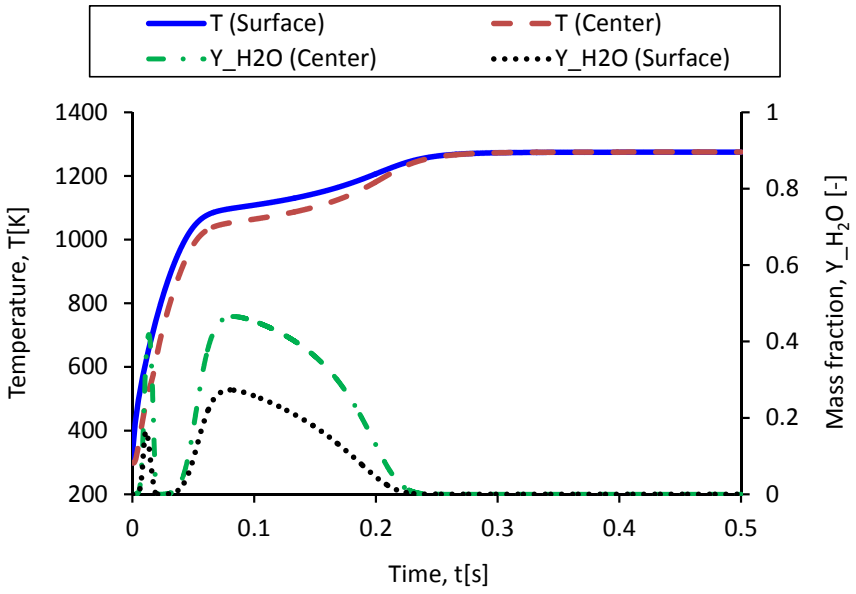

FIGURE 5.5: Model predicted profiles in temperature and water vapor at particle center/surface

As the clay particles experiences temperature gradient within the particle, it also displays a distinctly different mass fraction of water vapor across the particle radius. The two peaks observed on the above figure correspond to evaporation of free water and dehydroxylation, respectively. Since evaporation and dehydroxylation reactions are endothermic reactions, the energy demand by these reactions cause the temperature profile to be damped; at this instance, the the temperature and vapor mass fraction showed a clear gradient between the surface and center of the particle. Moreover, the intense release of water vapor during dehydroxylation gives rise to outward flow of vapor inside the solid matrix that offsets the inward heat conduction giving rise to maximum temperature difference between the particle surface and center during the two reaction periods.

Figure 5.6 illustrates the variation of kaolinite density as it transforms to metakaolinite and mullite. The density of kaolinite in the clay particle decreases as the dehydroxylation reaction starts. Kaolinite is completely depleted at the full dehydroxylation about 0.22 seconds, and transformed to metakaolinite. Further holding on the clay particle in

the hot air will lead to the transformation of metakaolinite into unwanted products, e.g., mullite. The particle conversion is deduced based on changes in particle mass. Accordingly, the conversion, X is computed as,

$$X = 1 - \frac{(m_{kl} + m_{fw})}{(m^0_{kl} + m^0_{fw})} \tag{5.1}$$

where, m_{kl} and m_{fw} represent the mass of kaolinite and free water in the clay particle at time t, while m^0_{kl} and m^0_{fw} denote their initial values in the raw clay particle, respectively.

As shown in Figure 5.6, the particle conversion is plotted against time. The clay particle attains complete conversion in about 0.22 seconds, at this time the clay product contains optimum amount of metakaolinite. The 14% of mass loss belongs to the amount of crystal water liberated during dehydroxylation.

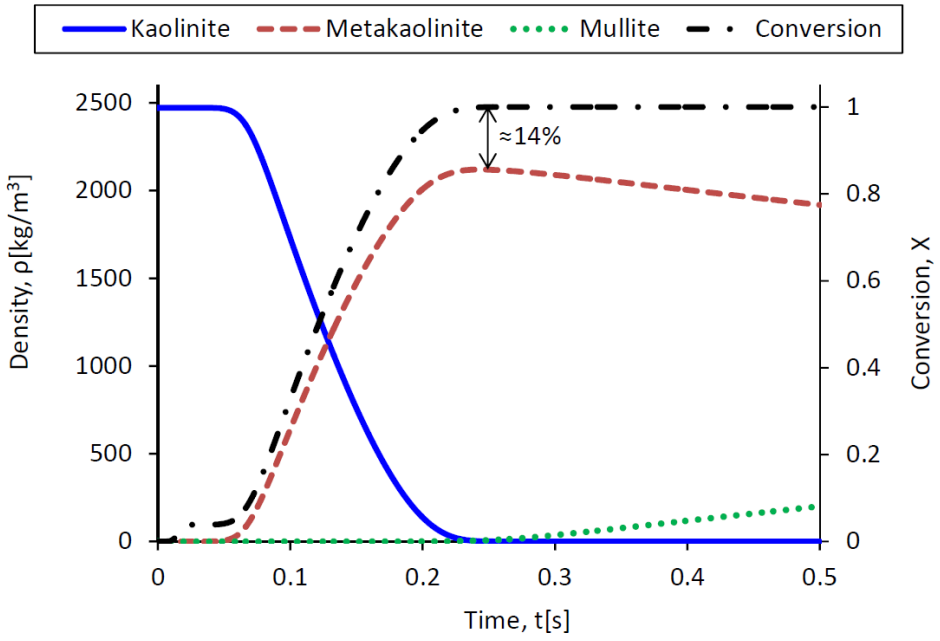

FIGURE 5.6: Model predicted density of solid species and conversion of the particle

The fact that koalinite undergoes a variation in density during flash calcination has been experimentally demonstrated [Davies, 1986; Slade and Davies, 1991]. The time at which the calcined product exhibit lower density has been assigned to the optimum amount of metakaolinite. According to Bridson et al. [1985], during calcination, kaolinite clay undergoes a change in density in a trend that depends on the degree of dehydroxylation. For such cases, an empirical trend is proposed as;

$$\rho = \rho_{kl}(1 - \beta\alpha) \tag{5.2}$$

where, ρ is the density of flash calcined product, ρ_{kl} is the density of the kaolinite sample, β is the mass ratio of water in the kaolinite sample ($\approx 14\%$) and α is the degree of dehydroxylation. The implication of this correlation is, for kaolinite clay having initial density 2630 kg/m^3, the calcined clay material could have a density as low as 2200 kg/m^3; provided that the volume of the clay material is assumed constant. In our model, using similar kaolinite properties such as, the density of kaolinite and β, as stated in Eq. 5.2, the same trend was observed in density as the empirical correlation established by Bridson et al. [1985]. In reality, flash calcines undergo a little swelling in volume and the density of the calcines is observed lower than the empirical trend. Flash calcination experiments carried out by Slade et al. [1992] are chosen for comparison purposes, where kaolinite clay sample is flash calcined at 1273 K for 0.5 seconds in nitrogen atmosphere. Different calcines are produced at different degrees of dehydroxylation by controlling the residence time. The calcines exhibit lower mean density than the suggested empirical trend; this is due to the presence of voids in their structure. Figure 5.7 illustrates the variation in density of kaolinite with degree of dehydroxylation for flash calcination experiments performed by Slade et al. [1992], the trend suggested by Bridson et al. [1985] and the model prediction. The agreement between model and the empirical trend is due to the assumption of negligible volume change during calcination.

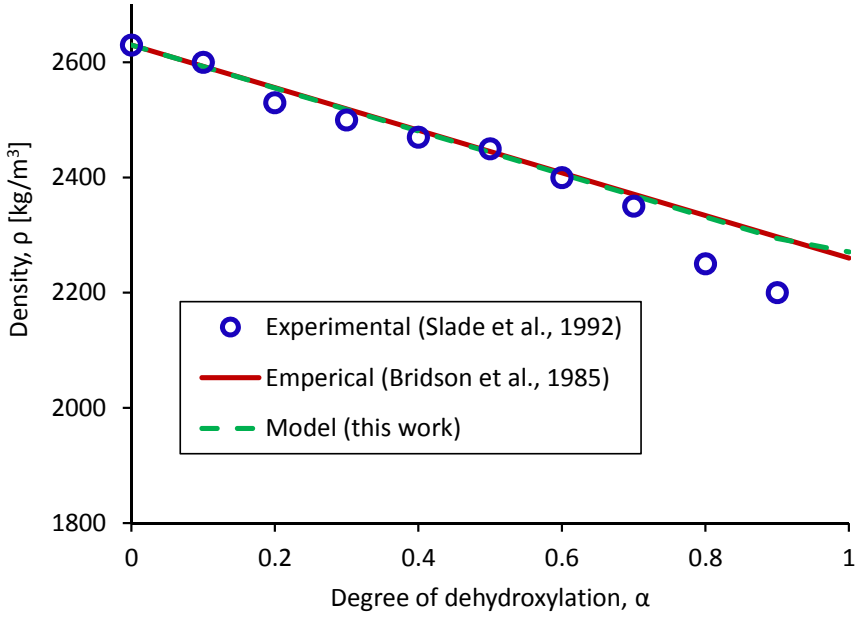

FIGURE 5.7: The changes in density of kaolinite as a function of degree of dehydroxylation during calcination: comparison between experiment, empirical correlation and model prediction.

In an attempt to locate the optimum amount of metakaolinite, Figure 5.8 illustrates the variation in density of the kaolinite model against time. The density of the calcined clay

products, ρ is calculated based on the mass fraction of individual solid species and their respective true density, which is given as,

$$\rho = \left(\sum_i \frac{Y_i}{\rho_i} \right)^{-1} \tag{5.3}$$

where, Y_i and ρ_i represent the mass fraction and material density of i^{th} solid component in the clay particle. The material densities used in this model are 2589, 2550, 3100, 2650, 2200 and 2270 kg/m^3 for kaolinite, metakaolinite, mullite, quartz, silica and cristobalite, respectively [Al-Akhras, 2006; Database, 2013].

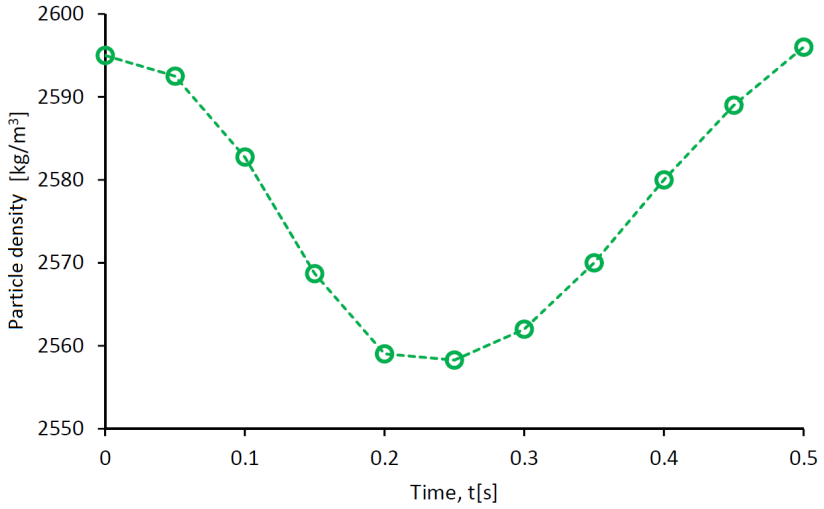

FIGURE 5.8: The variation in model predicted density of the calcined product as a function of time

It is evident from the graph above that for the calcination conditions specified above, most of the kaolinite particle gets dehydroxylated between 0.2–0.3 seconds. This observation is consistent with literature [Cadoret, 2005; Salvador and Davies, 1994].

The significance of convection, diffusion and chemical reaction during calcination has been examined for the particle model by using Peclet-Thiele mapping [Cardoso and Rodrigues, 2007; Lopes et al., 2009]. In order to assess the relative effect of chemical kinetics and mass transport through convection and diffusion, dimensionless parameters are used. Thiele modulus, ϕ is one of these parameters used for physical interpretation of the two time scales involved in the system; reaction and diffusion. Its value is computed as,

$$\phi = \frac{R_p}{3} \sqrt{\frac{S_g}{\varepsilon \rho_g D_{eff}}} \tag{5.4}$$

The influence of convection on the mass transfer of vapor can also be evaluated based on the Peclet mass transfer number, Pe_m which compares the ratio of convective to

diffusive mass transfer as:

$$Pe_m = \frac{R_p U}{3 D_{eff}} \tag{5.5}$$

The regime diagram suggested by Cardoso et al. [Cardoso and Rodrigues, 2007] and Lopes et al. [Lopes et al., 2013, 2009] is based on the values of Peclet and Thiele modules. Accordingly, the different regimes illustrated in Figure 5.9 characterize the interaction between chemical reaction, diffusion and intra-particle convection during the process. Thus, when the dominant phenomena are convection and diffusion, the flow is characterize by small values of Thiele modulus ($\phi^2/Pe_m \ll 1$). For smaller Peclet numbers ($Pe_m \ll 1$), and ($\phi^2 \approx 1$), diffusion and reaction are the dominant mechanisms. Intermediate values of the Thiele modulus ($\phi^2/Pe_m \approx 1$) illustrate convection and reaction are limiting during the process. As shown in the figure (dashed lines), the Pe_m values lie between 0 and 0.8 while the ϕ^2 values lie between 0 and 1.1. Thus, the flow regime of kaolinite dehydroxylation falls in the region where Diffusion-Convection-Reaction plays significant role. This ensures the importance of incorporating the diffusion, convection and reaction terms in the model. Based on the regime indicated for calcination process (dashed line) in the Figure 5.9, it can be generally suggested that diffusion is a dominant phenomena during calcination kaolinite rich clays. To be more specific, the small values of Thiele modulus ($0 \leq \phi^2 < 1.1$) and Peclet number ($0 \leq Pe_m < 0.8$) indicate convection, diffusion and reaction kinetics have a major impact during the process of thermal calcination, with diffusion being dominant over others.

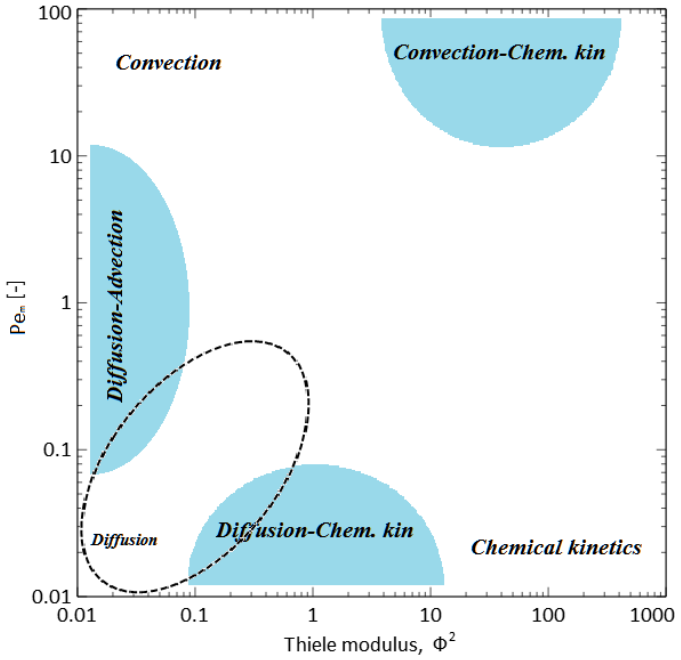

FIGURE 5.9: Regime diagram for convection, diffusion and chemical kinetics reproduced from Literature [Lopes et al., 2009] showing a specific region that belong to the calcination process of kaolinite clay (dashed line)

5.3.2 Sensitivity analysis

The parameter values and assumptions of any model are subject to change. The main aim of performing sensitivity analysis is to investigate the potential change of parameters and their impact on the conclusion to be drawn from the model. In this study, a sensitivity analysis is performed to examine the effect of calcination conditions (e.g., calcination temperature, time), clay particle properties (e.g., particle size) and some uncertain model inputs (e.g., kinetic parameters) on the final property of the calcined clay material. Detailed sensitivity analysis can be found in *Paper 3*.

Calcination temperature and time

As it is mentioned earlier, the thermal transformation of kaolinite into different phases is entirely dependent on calcination temperature. As the calcination temperature increase, there is high risk of formation of the undesired product called mullite that influence the pozzolanic property of the final product negatively. In order to investigate the sensitivity of calcination temperature on the property of the final product, the gas temperature has been varied from 1073 K to 1373 K and the impact on conversion profile is studied. Figure 5.10(A) depicts the effect of calcination temperature on the conversion of the kaolinite clay model. It is shown that, the higher the temperature, the faster the conversion to metakaolinite. However, the amount of metakaolinite is observed to be depleted as temperature and residence time increase. This is due to the transformation of metakaolinite into undesired phase. Figure 5.10(B) illustrates the impact of calcination temperature and residence time on the amount of metakaolinite. Thus, it is apparent that the right residence time and calcination temperature are extremely important to obtain maximum concentration of metakaolinite in the final calcined product.

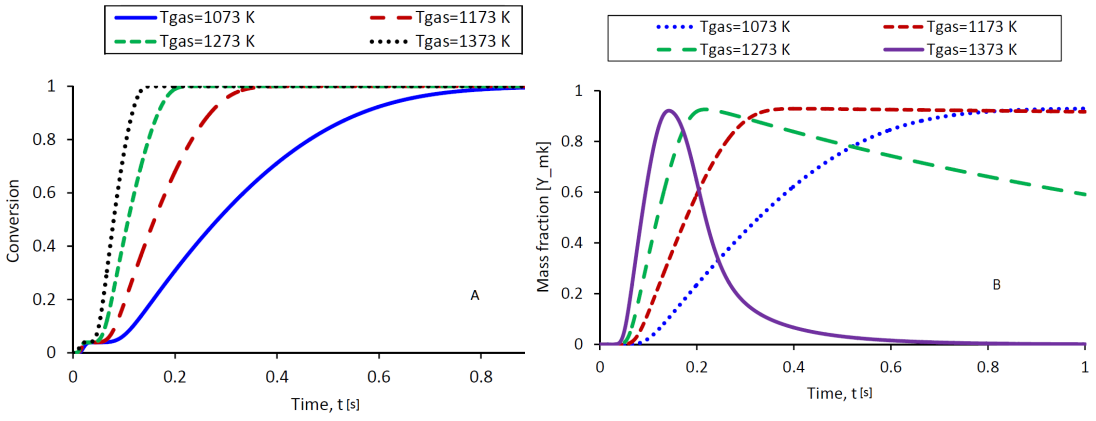

FIGURE 5.10: Sensitivity of calcination temperature and time on (A) model predicted conversion (B) model predicted mass fraction of metakaolinite

Particle size

Clay is composed of a number of tiny particles with several dimensions as shown in the experimental section. with this regard, sensitivity analysis on the particle size gives an overall idea on how the different particles behave during calcination. To investigate the effect of particle size on model results, different particle sizes that range from 25 µm to 150 µm are assumed and their impact on the conversion is studied. Figure 5.11 illustrates the impact of particle size on conversion.

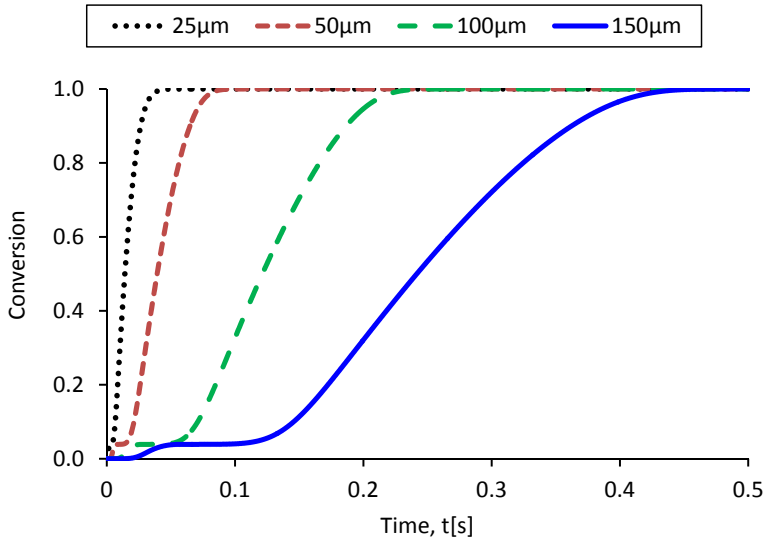

FIGURE 5.11: Sensitivity of particle size on model predicted conversion

As shown in the figure above, the conversion profile is a strong function of particle size. Thus, smaller particles are observed to attain full conversion rapidly, whereas larger particles of diameter 150 µm, the intra-particle heat and mass transfer resistances become more important than the external heat and mass transfer resistance and this delays the time of full conversion.

Kinetic parameters

Since the expression of reaction rates is based on Arrhenius type of dependence which is interpreted in terms of kinetic parameters (E and A), the influence of these parameters on thermal calcination of the kaolinite model is unquestionable. A number of kinetic parameters have been reported in the literature, specially for dehydroxylation reaction step. Table 5.4 summarizes some selected values of kinetic parameters given for dehydroxylation of kaolinite from the literature.

TABLE 5.4: A summary of kinetic parameters for kaolinite dehydroxylation from literature

E(kJ/mol)	A($s^{-}1$)	Method	Source	Reference
177	4.57×10^{8}	Thermal Analysis, DTA	Florida, USA	[Kissinger, 1956]
193	1.0×10^{9}	Thermal Analysis, TGA	Georgia, USA	[Bellotto et al., 1995]
196	9.6×10^{8}	Thermal Analysis, TGA	India	[Saikia et al., 2002]
195	8.58×10^{14}	Thermal Analysis, DTG	Rep. Czech	[Ptáček et al., 2011]
163	2.0×10^{12}	Thermal Analysis, TGA	USA	[Levy and Hurst, 1993]
180	6.3×10^{9}	Thermal Analysis, TGA	EU	this work

Here, the influence of the above mentioned kinetic parameters on the degree of conversion of kaolinite model has been investigated and compared with the experimentally determined kinetic parameters in this study. Figure 5.12 illustrates the impact of kinetic parameters on the conversion profile of the model. Consequently, the sensitivity of kinetic parameters can be judged from the different conversion profiles observed in the figure.

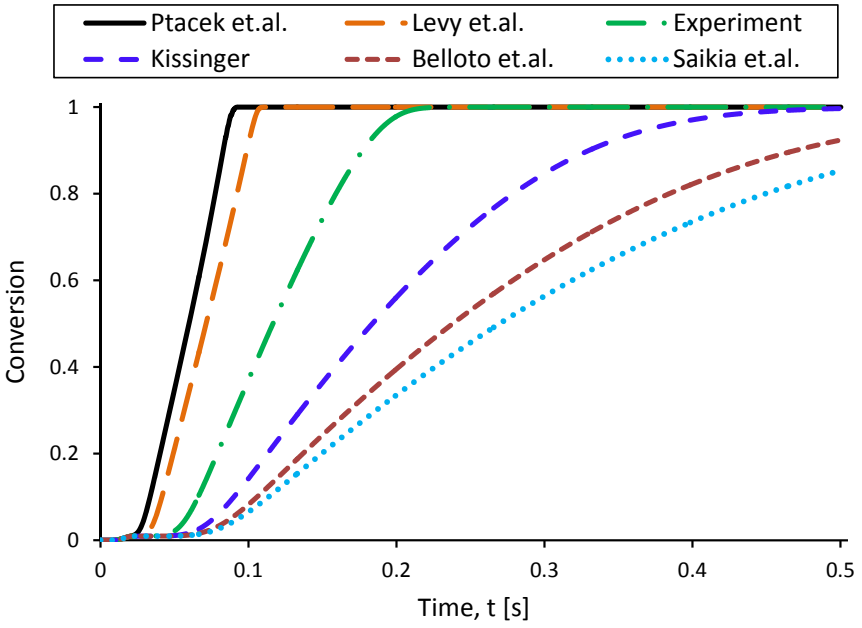

FIGURE 5.12: The sensitivity of kinetic parameters based on literature and their impact on the conversion profile of the model

Chapter 6

Conclusion

This section brings the summary and conclusions made out of the study. Recommendations are also made to further improve the existing research work based on more reliable inputs and suggestions on the particle model.

6.1 Final remarks

Thermal calcination of kaolinite has been of current interest in cement and concrete industry. Based on its application for the intended use, the calcined material needs to have high concentration of the pozzolanic active material, metakaolinite. Besides, flash calcined metakaolinite displays typical properties that enhance the materials pozzolanic property. As flash calcination is a very quick process that could yield a calcined product in a fraction of seconds, modeling of such processes enable us to capture and understand the inter-particle processes during transformation.

In this work, thermal calcination kaolinite rich clay particles is studied by using both modeling and experimental approaches. Both modeling and experimental results show a good agreement.

A comprehensive mathematical model has been successfully developed for clay particle calcination, which sufficiently addresses the key intra-particle processes and the particle-ambient flow interaction. The model reliably predicts favorable production path that may able to achieve an optimum amount of the desired product, namely metakaolinite. Based on the kinetic, physical and thermodynamic data used in the model, when kaolinite rich clay particles are plunged into a hot gas atmosphere, the clay particles are observed to dehydroxylate quickly. The speed at which the kaolinite clay is converted into metakaolinite depends on the calcination temperature, particle size and other inputs

such as kinetic parameters. Simulation of kaolinite particle model in different calcination temperature has predicted interesting results that may give a full picture on the operation conditions of a flash calciner. Generally, there are three entirely correlated factors that may influence the process: calcination temperature, particle size and the yield of metakaolinite. In order to achieve optimum amount of metakaolinite, a compromise is important among the above parameters. Clay particles exposed to high calcination temperatures (>1273 K) may exhibit not only faster conversion but also faster phase transformation into undesired material. Again, lower temperatures (<1073 K) may require longer residence time and may not have the risk of phase transformation. Based on these observations, calcination temperatures 1173 K–1273 K may hold a reasonable tradeoff in the amount of metakaolinite and residence time. At such calcination temperatures, even though the model predicts lower residence time (0.2 – 0.3 s), when calcination continues for half a second (0.5 s) the calcined material still contains sufficient amount of metakaolinite enough to be used as an input in concrete production.

From the modeling perspective, the physical and thermodynamic properties that characterize clay particles are found to limit simulation results. The complex nature of clays is also another factor that may result in diverse values of kinetic parameters. The sensitivity analysis on kinetic parameters revealed the influence on dehydroxylation process. In such cases of uncertainty, tuning the kinetic parameters based on experimental results can provide a good estimation of their values.

Flash calcination experiments in a gas suspension calciner are presented for a residence time of 0.5 seconds. Under different calcination temperatures, the composition of the calcined material is experimentally examined. In all cases, the calcined product is observed to comprise high amount of the required material, metakaolinite. Yet, optimum amount of metakaolinite is noticed at higher temperatures; except for temperatures at 1273 K in the presence of secondary burners. This observation is in agreement with model prediction. However, the need for a stable temperature inside the calciner is important to mention.

6.2 Future work

As there is only a little work reported in the literature about modeling calcination of kaolinite clay, some recommendations that might help to further improve the results of this study are described below.

In order to gain more fundamental insight on the calcination process, the reaction rate on the more influencing reaction step, which is dehydroxylation, might need more refinement

and better expression. Owing to the sensitivity of the calcination process towards kinetic parameters and the difficulty of determining these variables, as briefly stated in this work, rate expressions that are based on Arrhenius equation could contribute to the major share for such uncertainties. A new paradigm shift may be necessary in expressing the reaction rates for solid-gas reactions as described in [Favergeon et al., 2013; Michèle et al., 2011]. These expressions may somehow solve the doubts on predicted properties that vary significantly with kinetic parameters.

From the perspective of the particle model, the first question that might appear could be whether one dimensional approach is sufficient to model the complex structure and nature of clays. Two dimensional or fully three dimensional structure of kaolinite clay particles could be more appropriate to address the intra-particle transport phenomenon and any structural change, if proper description of particle shape is available.

In the entire SCM project, a lot of good efforts are made on the processes at the downstream side of the calciner, e.g., comprehensive characterization of the calcines obtained under various calcination condition, and concrete tests by using the calcined clay in concrete. In this thesis, models for single clay particle calcination are successfully developed and validated. However, all these are far from being enough, in terms of cost-effective innovative design of smart, energy-efficient large-scale gas suspension clay calciners. To achieve this, advanced CFD simulation of the reacting particulate flow system in the calciner must be performed, in which all the highly coupled sub-processes (e.g., complicated particulate flow, heat transfer, clay particle conversion, particle agglomeration and so on) must be appropriately addressed. The CFD simulation of the entire calciner must be somehow validated (e.g., by experimental data) to assure that a reliable CFD modeling capability for such a gas suspension flash calcination process is established. Only after that, a true understanding of the details in the calciner and the impacts of various factors can be reliably achieved (e.g., via CFD model-based sensitivity study), and smart, energy-efficient large-scale gas suspension calciners can be designed and optimized in a reliable and cost-effective way (i.e., mainly based on the CFD capability, with proper combination of experience and a few tests and adjustment).

Bibliography

Abramzon, B. and W. Sirignano (1989). Droplet vaporization model for spray combustion calculations. *Int. J. Heat Mass Transf. 32*(9), 1605–1618.

Al-Akhras, N. (2006). Durability of metakaolin concrete to sulfate attack. *Cem. Concr. Res. 36*, 1727–1734.

Allison, E. (1955). Quantitative thermal analysis of clay minerals. *Clay Miner. Bull 2*, 242–254.

Ambroise, J., M. Murat, and J. Péra (1985). Hydration reaction and hardening of calcined clays and related minerals. V. Extension of the research and general conclusions. *Cem. Concr. Res. 15*, 261–268.

Arikan, M., K. Sobolev, T. Ertün, A. Yeğinobali, and P. Turker (2009). Properties of blended cements with thermally activated kaolin. *Constr. Build. Mater. 23*(1), 62–70.

Augis, J. and J. Bennett (1978). Calculation of the Avrami parameters for heterogeneous solid state reactions using a modification of the Kissinger method. *J. Therm. Anal. Calorim. 13*, 283–292.

Baumann, W., A. Leineweber, and E. J. Mittemeijer (2010). Failure of Kissinger (-like) methods for determination of the activation energy of phase transformations in the vicinity of the equilibrium phase-transformation temperature. *J. Mater. Sci. 45*(22), 6075–6082.

Bellotto, M., A. Gualtieri, G. Artioli, and S. Clark (1995). Kinetic study of the kaolinite-mullite reaction sequence. Part I: kaolinite dehydroxylation. *Phys. Chem. Miner. 22*, 207–214.

Benitez, J. (2009). *Principles and modern applications of mass transfer operations* (Second ed.). New jersy: John willey & sons.

Bergman, T., A. Lavine, F. Incropera, and D. DeWitt (2011). *Fundamentals of heat and mass transfer* (Seventh ed.). Jefferson city, USA: Jonh Wiley & Sons.

Bhatia, S. (1985). On the pseudo steady state hypothesis for fluid solid reactions. *Chem. Eng. Sci. 40*(5), 868–882.

Bish, D. and J. Post (1993). Quantitative mineralogical analysis using the Rietveld full-pattern fitting method. *Am. Mineral. 78*, 932–940.

Bolz, R. and G. Tuve (1976). *Handbook of Tables for Applied Engineering Science* (Second ed.). New York: CRC press.

Borgwardt, R. H. (1985). Calcination kinetics and surface area of dispersed limestone particles. *AIChE J. 31*(1), 103–111.

Boswell, P. (1980). On the calculation of activation energies using a modified Kissinger method. *J. Therm. Anal. Calorim. 18*, 353–358.

Bridson, D., T. Davies, and D. Harrison (1985). Properties of flash-calcined kaolinite. *Clays Clay Miner. 33*(3), 258–260.

Brindley, G. and M. Nakahira (1958). A new concept of the transformation sequence of kaolinite to mullite. *Nature* (4619), 1333–1334.

Brindley, G., J. Sharp, J. Petterson, and B. Narahari (1967). Mechanism of dehydroxylation processes, I. Temperature and vapor pressure dependence of dehydroxylation of kaolinite. *Am. Mineral. 52*(65), 201–211.

Bryden, K. M. and M. J. Hagge (2003). Modeling the combined impact of moisture and char shrinkage on the pyrolysis of a biomass particle. *Fuel 82*(13), 1633–1644.

Cabrera, J. and M. Eddleston (1983). Kinetics of dehydroxylation and evaluation of the crystallinity of kaolinite. *Thermochim. Acta 70*, 237–247.

Cadoret, G. (2005). Dehydroxylated aluminium silicate based material, process and installation for the manufacture thereof, US patent 2005/0039637 A1, Feb. 24, 2005.

Cardoso, S. S. and A. E. Rodrigues (2007). Convection, diffusion and reaction in a nonisothermal, porous catalyst slab. *AIChE journal 53*(5), 1325–1336.

Cassagnabère, F., M. Mouret, G. Escadeillas, P. Broilliard, and A. Bertrand (2010). Metakaolin, a solution for the precast industry to limit the clinker content in concrete: Mechanical aspects. *Constr. Build. Mater. 24*(7), 1109–1118.

Chen, D., X. Gao, and D. Dollimore (1993). A generalized form of the Kissinger equation. *Thermochim. Acta 215*, 109–117.

Chen, Y., M. Wang, and M. Hon (2003). Transformation kinetics for mullite in kaolin-Al2O3 ceramics. *J. Mater. Res 18*(6), 1355–1362.

Chung, F. H. and D. K. Smith (1999). *Industrial Applications of X-Ray Diffraction.* NY, USA: CRC Press.

Criado, J., A. Ortega, C. Real, and E. Torres De Torres (1984). Re-Examination of the Kinetics of the Thermal Dehydroxylation of Kaolinite. *Clay Miner. 19*(4), 653–661.

Dam, T. (2013). Supplementary Cementitious Materials and Blended Cements to Improve Sustainability of Concrete Pavements. *Natl. Concr. Pavement Technol. Center. Iowa state Univ.*, http://www.cptechcenter.org/technical–library/docu, online: accessed on March 2014.

Database (2013). Mineralogic database-Mineral Collecting, Localities, Mineralogy database-Mineral Photos and Data. http://www.mindat.org/, Accessed on January, 2013.

Davies, T. (1986). Flash dehydroxylation of kaolinite: the effect of heating rate on the properties of the calcine. *J. Mater. Sci. Lett. 5*, 186–187.

Diamond, S. (1970). Pore Size Distributions in Clays. *Clays Clay Miner. 18*(1), 7–23.

Dion, P., J. Alcover, F. Bergaya, A. Ortega, P. L. Llewellyn, and F. Rouquerol (1998). Kinetic study by controlled-transformation rate thermal analysis of the dehydroxylation of kaolinite. *Clay Miner. 33*(2), 269–276.

Favergeon, L., J. Morandini, M. Pijolat, and M. Soustelle (2013). A General Approach for Kinetic Modeling of Solid-Gas Reactions at Reactor Scale: Application to Kaolinite Dehydroxylation. *Oil Gas Sci. Technol. – Rev. IFP Energies Nouv. 68*(6), 1039–1048.

Fernandez, R., F. Martirena, and K. L. Scrivener (2011). The origin of the pozzolanic activity of calcined clay minerals: A comparison between kaolinite, illite and montmorillonite. *Cem. Concr. Res. 41*(1), 113–122.

Fidaros, D., C. Baxevanou, C. Dritselis, and N. Vlachos (2007). Numerical modelling of flow and transport processes in a calciner for cement production. *Powder Technol. 171*(2), 81–95.

Georgakis, C., C. Chang, and J. Szekely (1979). A changing grain size model for gas—solid reactions. *Chem. Eng. Sci. 2*(4), 1072–1075.

Gerardin, C. and S. Sundaresan (1994). Structural investigation and energetics of mullite formation from sol-gel precursors. *Chem. Mater. 6*(2), 160–170.

Grim, R. E. (1953). *Clay mineralogy.* New York: McGRAW-HILL.

Hankock, J. D. and J. H. Sharp (1972). Method of Comparing Solid-State Kinetic Data and Its Application to the Decomposition of Kaolinite, Brucite, and BaCO3. *J. Am. Ceram. Soc. 55*(2), 74–77.

He, C., E. Makovicky, and B. Osbæ ck (1994). Thermal stability and pozzolanic activity of calcined kaolin. *Appl. Clay Sci. 9*, 165–187.

Hewlett, P. (1998). *Lea' s Chemistry of Cement and Concrete* (4th ed.). Burlington, USA: Elsevier Science and Technology Books.

Holm, J. (2001). Kaolinites–mullite transformation in different Al2O3–SiO2 systems: Thermo-analytical studies. *Phys. Chem. Chem. Phys.*, 10–13.

Holm, J., O. Kleppa, and E. Westrum (1967). Thermodynamics of polymorphic transformations in silica. Thermal properties from 5 to 1070 K and pressure-temperature stability fields for coesite and stishovite. *Geochim. Cosmochim. Acta 31*, 2289–2307.

Horvath, I. (1985). Kinetics and Compensation effect in kaolinite Dehydroxylation. *Thermochem. Acta 85*, 193–198.

Hu, N. and A. W. Scaroni (1996). Calcination of pulverized limestone particles under furnace injection conditions. *Fuel 75*(2), 177–186.

Humphreys, K. and M. Mahasenan (2002). Towards a sustainable cement industry substudy 8: climate change. *http://www.wbcsdcement.org/pdf/battelle/final_report8.pdf*, Online; accessed march 2014.

IEA (2009). Cement Technology Roadmap 2009. International Energy Agency (IEA)/World Business Council for Sustainable Development(WBCSD) report. Technical report.

Khatib, J., E. Negim, and E. Gjonbalaj (2012). High volume metakaolin as cement replacement in mortar. *World J. Chem. 7*(1), 7–10.

Kissinger, H. (1957). Reaction kinetics in differential thermal analysis. *Anal. Chem. 29*, 1702–1706.

Kissinger, H. E. (1956). Variation of peak temperature with heating rate in differential thermal analysis. *J. Res. Natl. Bur. Stand. (1934). 57*(4), 217–21.

Knovel (2013). Technical engineering reference information, http://why.knovel.com/, accessed on july, 2013.

Lahiri, A. (1980). The effect of particle size distribution on TG. *Thermochim. Acta 40*, 289–295.

Levy, J. and H. Hurst (1993). Kinetics of dehydroxylation, in nitrogen and water vapour, of kaolinite and smectite from Australian Tertiary oil shales. *Fuel 72*(6), 873–877.

Li, C., H. Sun, and L. Li (2010). A review: The comparison between alkali-activated slag (Si+Ca) and metakaolin (Si+Al) cements. *Cem. Concr. Res. 40*(9), 1341–1349.

Llópiz, J., M. Romero, A. Jerez, and Y. Laureiro (1995). Generalization of the Kissinger equation for several kinetic models. *Thermochim. Acta 256*, 205–211.

Lopes, J., M. Alves, M. Oliveira, S. Cardoso, and A. Rodrigues (2013). Internal mass transfer enhancement in flow-through catalytic membranes. *Chem. Eng. Sci. 104*, 1090 – 1106.

Lopes, J., S. Cardoso, and A. Rodrigues (2009). Convection, diffusion, and exothermic zero order reaction in a porous catalyst slab: Scaling and perturbation analysis. *AIChE J. 55*(10).

Lothenbach, B., K. Scrivener, and R. Hooton (2011). Supplementary cementitious materials. *Cem. Concr. Res. 41*(12), 1244–1256.

Lu, H., W. Robert, G. Peirce, B. Ripa, and L. L. Baxter (2008). Comprehensive Study of Biomass Particle Combustion. *Energy & Fuels 22*(4), 2826–2839.

Massazza, F. (1993). Pozzolanic cements. *Cem. Concr. Compos. 15*(1993), 185–214.

Mehta, B. Y. P. K. (2002). Greening of the Concrete Industry for Sustainable Development. *Concr. Int.*, 23–28.

Meinhold, R., H. Atakul, and T. Davies (1992). Flash calcines of kaolinite: kinetics of isothermal dehydroxylation of partially dehydroxylated flash calcines and of flash calcination itself. *J. Mater. Chem. 38*(9), 913–921.

Meinhold, R. and S. Salvador (1994). A comparison of the kinetics of flash calcination of kaolinite in different calciners. *IChemE 72*(part A), 105–113.

Michèle, P., F. Loïc, and S. Michel (2011). From the drawbacks of the Arrhenius-f(α) rate equation towards a more general formalism and new models for the kinetic analysis of solid–gas reactions. *Thermochim. Acta 525*(1-2), 93–102.

Michot, A., D. S. Smith, S. Degot, and C. Gault (2008). Thermal conductivity and specific heat of kaolinite: Evolution with thermal treatment. *J. Eur. Ceram. Soc. 28*(14), 2639–2644.

Mikulčić, H., E. von Berg, M. Vujanović, P. Priesching, L. Perković, R. Tatschl, and N. Duić (2012). Numerical modelling of calcination reaction mechanism for cement production. *Chem. Eng. Sci. 69*(1), 607–615.

Murray, H. H. (1963). Industrial applications of kaolin. In *Tenth Natl. Conf. clays clay Miner.*, pp. 291–298.

Murray, P. and J. White (1955). Kinetics of clay dehydration. *Clay Min. 2*, 255–264.

Oh, M. and C. Pantelides (1996). A modelling and simulations language for combined lumped and distributed parameter systems. *Comput. chem.Engng 20*, 661–633.

Opfermann, J. and H. Flammersheim (2003). Some comments to the paper of JD Sewry and ME Brown:"Model-free" kinetic analysis? *Thermochim. Acta 397*, 1–3.

Ortega, A., M. Macias, and F. J. Gotor (2010). The Multistep Nature of the Kaolinite Dehydroxylation: Kinetics and Mechanism. *J. Am. Ceram. Soc. 93*(1), 197–203.

Pantelides, C. and P. Barton (1993). Equation-oriented dynamic simulation current status and future perspectives. *Comput. Chem. Eng. 17*, S263–S285.

Patankar, S. v. (1980). *Numerical heat transfer and fluid flow.* USA: Hemispher Publishing Corporation.

Patisson, F., M. G. François, and D. Ablitzer (1998). A non-isothermal, non-equimolar transient kinetic model for gas-solid reactions. *Chem. Eng. Sci. 53*(4), 697–708.

Pijolat, M., F. Valdivieso, and M. Soustelle (2005). Experimental test to validate the rate equation "dα/dt=kf(α)" used in the kinetic analysis of solid state reactions. *Thermochim. Acta 439*(1-2), 86–93.

Prasad, M., K. Reid, and H. Murray (1991). Kaolin: processing, properties and applications. *Appl. Clay Sci. 6*(2), 87–119.

PSE (2013). gPROMS Model Developer's Guide, www.psenterprise.com.

Ptáček, P., M. Křečková, F. Šoukal, T. Opravil, J. Havlica, and J. Brandštetr (2012). The kinetics and mechanism of kaolin powder sintering I. The dilatometric CRH study of sinter-crystallization of mullite and cristobalite. *Powder Technol. 232*, 24–30.

Ptáček, P., F. Šoukal, T. Opravil, J. Havlica, and J. Brandštetr (2011). The kinetic analysis of the thermal decomposition of kaolinite by DTG technique. *Powder Technol. 208*(1), 20–25.

Ptáček, P., F. Šoukal, T. Opravil, M. Nosková, J. Havlica, and J. Brandštetr (2010). The non-isothermal kinetics analysis of the thermal decomposition of kaolinite by Effluent Gas Analysis technique. *Powder Technol. 203*(2), 272–276.

Ranz, W. and W. Marshall (1952). Evaporation from drops. *Chem. Eng. Prog. 48*, 141–146.

Redfern S. (1987). kinetics of kaoline dehydroxyaltion of kaolinite. *Clay Miner. 22*, 447–456.

Rehan, R. and M. Nehdi (2005). Carbon dioxide emissions and climate change: policy implications for the cement industry. *Environ. Sci. Policy 8*(2), 105–114.

Reinecke, S. and B. E. Sleep (2002). Knudsen diffusion, gas permeability, and water content in an unconsolidated porous medium. *Water Resour. Res. 38*(12), 1–15.

Robie, R. A., B. S. Hemingway, and J. R. Fisher (1979). *Thermodynamic Properties of Minerals and Related Substances at 298.15 K and 1bar pressure and at higher temperatures*. Washington D.C: United states government printing office.

Sabir, B., S. Wild, and J. Bai (2001). Metakaolin and calcined clays as pozzolans for concrete: a review. *Cem. Concr. Compos. 23*(6), 441–454.

Said-Mansour, M., E.-H. Kadri, S. Kenai, M. Ghrici, and R. Bennaceur (2011). Influence of calcined kaolin on mortar properties. *Constr. Build. Mater. 25*(5), 2275–2282.

Saikia, N., P. Sengupta, P. K. Gogoi, and P. C. Borthakur (2002). Kinetics of dehydroxylation of kaolin in presence of oil field effluent treatment plant sludge. *Appl. Clay Sci. 22*(3), 93–102.

Salvador, S. (1995). Pozzolanic properties of flash-calcined kaolinite: a comparative study with soak-calcined products. *Cem. Concr. Res. 25*(1), 102–112.

Salvador, S. and T. Davies (1994). Modeling of combined heating and dehydroxylation of kaolinite particles during flash calcination; production of metakaolinite. *Process. Adv. Mater. 9*, 128–135.

San Nicolas, R., M. Cyr, and G. Escadeillas (2013). Characteristics and applications of flash metakaolins. *Appl. Clay Sci. 83-84*, 253–262.

Schilling, M. (1990). Effects of sample size and packing in the thermogravimetric analysis of calcium montmorillonite STx-1. *Clays Clay Miner. 38*(5), 556–558.

Sesták, J., P. Holba, and Z. Zivkovic (2014). Doubts on Kissingers method of kinetic evaluation based on several conceptual models showing the difference between the maximum of reaction rate and the extreme of a DTA peak. *J. Min. Metall. Sect. B Metall. 50*(1), 77–81.

Sharp, J. H., G. W. Brindley, and B. N. N. Achar (1966). Numerical Data for Some Commonly Used Solid State Reaction Equations. *J. Am. Ceram. Soc. 49*(7), 379–382.

Shehata, M. and M. Thomas (2002). Use of ternary blends containing silica fume and fly ash to suppress expansion due to alkali–silica reaction in concrete. *Cem. Concr. Res. 32*, 341–349.

Shvarzman, A., K. Kovler, G. Grader, and G. Shter (2003). The effect of dehydroxylation/amorphization degree on pozzolanic activity of kaolinite. *Cem. Concr. Res. 33*(3), 405–416.

Silcox, G. D., J. C. Kramlich, and D. W. Pershing (1989). A Mathematical model for the flash calcination of dispersed CaCO3 and Ca(OH)2 particles. *Ind. Eng. Chem. Res. 28*, 155–160.

Slade, R. and T. Davies (1991). Evolution of Structural Changes during Flash Calcination of Kaolinite. *Mater. Chem. 1*(3), 361–364.

Slade, R., T. Davies, and H. Atakül (1991). Flash calcination of kaolinite: mechanistic information from thermogravimetry. *J. Mater. Chem. 1*(5), 751–756.

Slade, R., T. Davies, H. Atakül, and R. Hooper (1992). Flash calcines of kaolinite: effect of process variables on physical characteristics. *J. Mater. Sci. 27*, 2490–2500.

Snellings, R., L. Machiels, G. Mertens, and J. Elsen (2010). Rietveld Refinement strategy for quantitative Phase analysis of partially amorphous zeolitized tuffaceous rocks. *Geol. Belgica 13*, 183–196.

Stoch, L. (1984). Significance of structural factors in dehydroxylation of kaolinite polytypes. *J. Therm. Anal. 29*(5), 919–931.

Stoch, L. and I. Waclawska (1981). Dehydroxylation of kaolinite group minerals I. Kinetics of dehydroxylation of kaolinite and halloysite. *J. Therm. Anal. 20*, 291–304.

Szekely, J. and M. Propster (1975). A structural model for gas-solid reactions with a moving boundary -VI. *Chem. Eng. Sci. 30*, 1049–1055.

Takkinen, S., J. Saastamoinen, and T. Hyppänen (2012). Heat and mass transfer in calcination of limestone particles. *AIChE J. 58*(8), 2563–2572.

Tavman, I. (1996). Effective thermal conductivity of granular porous materials. *Int. Commun. Heat Mass Transf. 23*(2), 169–176.

Thomas, M., M. Shehata, S. Shashiprakash, D. Hopkins, and K. Cail (1999). Use of ternary cementitious systems containing silica fume and fly ash in concrete. *Cem. Concr. Res. 29*(8), 1207–1214.

Tikalsky, P. J., M. V. Huffman, and G. M. Barger (2001). Use of Raw or Processed Natural Pozzolans in Concrete. *Am. Concr. Inst.*, 1–24.

Tironi, A., M. A. Trezza, A. N. Scian, and E. F. Irassar (2012). Kaolinitic calcined clays: Factors affecting its performance as pozzolans. *Constr. Build. Mater. 28*(1), 276–281.

Versteeg, H. and W. Malalasekera (2007). *An introduction to computational fluid dynamics* (Second ed.). Essex: Pearson Education Limited.

Weber, J. N. and R. Roy (1965). Dehydroxylation of kaolinite, Dickite and Halloysite: Heats of reaction and kinetics of dehydration at PH2O=15psi. *Am. Mineral. 50*, 1038–45.

Wen, C. and S. Wang (1970). Thermal and Diffusional Effects Solid Gas Reactions. *Ind. Eng. Chem. 62*, 30–51.

Yin, C., K. Kaer, L. Rosendahl, and L. Hvid (2010). Co-firing straw with coal in a swirl-stabilized dual-feed burner: modelling and experimental validation. *Bioresour. Technol. 101*(11), 4169–78.